American Mineralogist, Volume 81, pages 525–544, 1996

Pyroxene as a recorder of cumulate formational processes in asteroids, Moon, Mars, Earth: Reading the record with the ion microprobe*

J.J. Papike

Institute of Meteoritics, Department of Earth and Planetary Sciences, University of New Mexico, Albuquerque, New Mexico 87131-1126, U.S.A.

Abstract

Igneous cumulate rocks provide an important record of planetary magmatism, but there are pitfalls in their interpretation. Cumulus minerals may react with the trapped melt and other cumulus phases during subsolidus reactions, thus losing a direct record of their igneous history. One of the best approaches for estimating the melt compositions parental to the cumulates is to analyze the cores of cumulus phases for elements with slow diffusion rates (e.g., REE in pyroxene) because these most reliably retain a record of the mineral-melt partitioning. We have conducted SIMS studies of pyroxenes from a variety of planetary cumulates, including lunar norites, martian orthopyroxenites, asteroidal orthopyroxenites (diogenites), asteroidal pyroxene-plagioclase cumulates (cumulate eucrites), and terrestrial orthopyroxenites and norites (Stillwater Complex, Montana). We emphasized the REE (La, Ce, Nd, Sm, Eu, Dy, Er, Yb) along with Sr, Y, and Zr in these investigations. Our studies yielded the several conclusions. (1) Lunar Mg-suite norites crystallized from highly evolved (KREEPy) melts that were emplaced into the lunar anorthositic crust. One viable model suggests remobilization of KREEP lithologies that formed late in the crystallization of the lunar magma ocean. (2) Orthopyroxenites from asteroid 4 Vesta (diogenites) likely formed as cumulates from melts derived from depleted mantle, which had previously experienced eucritic basalt removal. The calculated parental melts show a limited range of major element compositions but an exceedingly large range of trace element variation that is difficult to explain by any simple crystallization or melting models. (3) The diogenites of 4 Vesta are cumulates from melts derived from many depleted mantle reservoirs that either formed numerous orthopyroxene plutons, later mixed by impact brecciation, or commingled by magma mixing to form a limited number of differentiated plutons. We base this conclusion on a comparative investigation of a well-studied terrestrial orthopyroxenite sequence (Bronzitite zone of the Stillwater Complex).

An important lesson to be learned from these studies in comparative planetology is that if simple petrogenetic models do not work for well-studied terrestrial occurrences there is little reason to believe that they will work for planetary environments where we have little geologic control on sampling.

Introduction

A fundamentally important process that occurred in all the terrestrial planets and some asteroids is magmatism, and we seek to understand the details of this process that are unique to individual planetary bodies. Only in rare cases does the melt derived from melting of a planetary mantle arrive at a planetary surface without the loss of some crystals. Usually separation and accumulation of crystals take place, forming cumulate rocks. Interpretation of these important lithologies is not straightforward, and aspects that must be considered when studying such rocks are nicely summarized by Barnes (1986): "Three principal factors must be taken into account when interpreting mineral compositions in cumulate rocks: (1) changes in the composition of the parent magma due to fractional crystallization, contamination, magma mixing, etc.; (2) superimposed modification of mineral compositions as a result of crystallization of trapped intercumulus liquid; (3) redistribution of elements due to subsolidus reequilibration between minerals."

An approach that minimizes some of these interpretive problems is to analyze the cores of cumulus minerals for elements with slow diffusion rates (e.g., REE, Y, Zr). For cumulate rocks pyroxene is an especially powerful recorder of magmatic processes (Fig. 1). Lambert and Simmons (1987) used this approach by attempting to analyze the cores of orthopyroxene grains by using an abrasion technique to remove the rims. Now, with the develop-

* Adapted from the Presidential Address given at the annual meeting of the Mineralogical Society of America, November 7, 1995, in New Orleans, Louisiana.

0003–004X/96/0506–0525$05.00

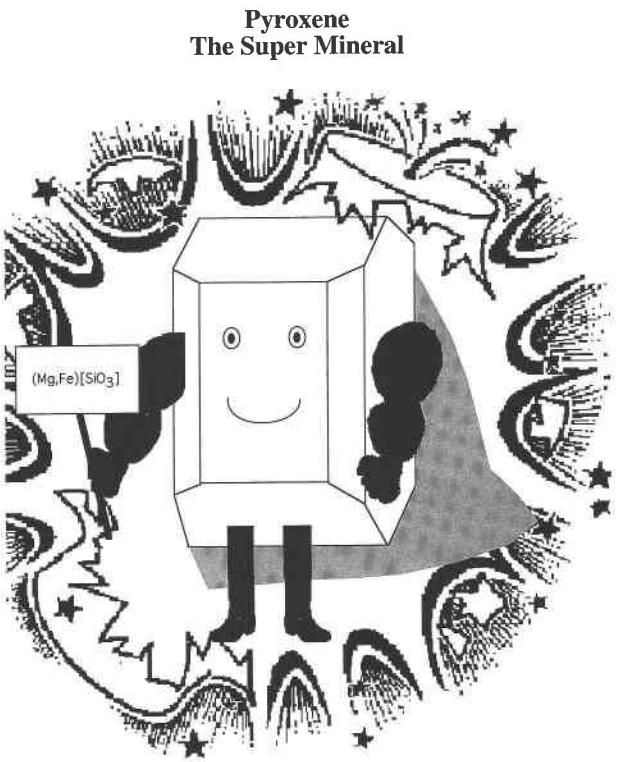

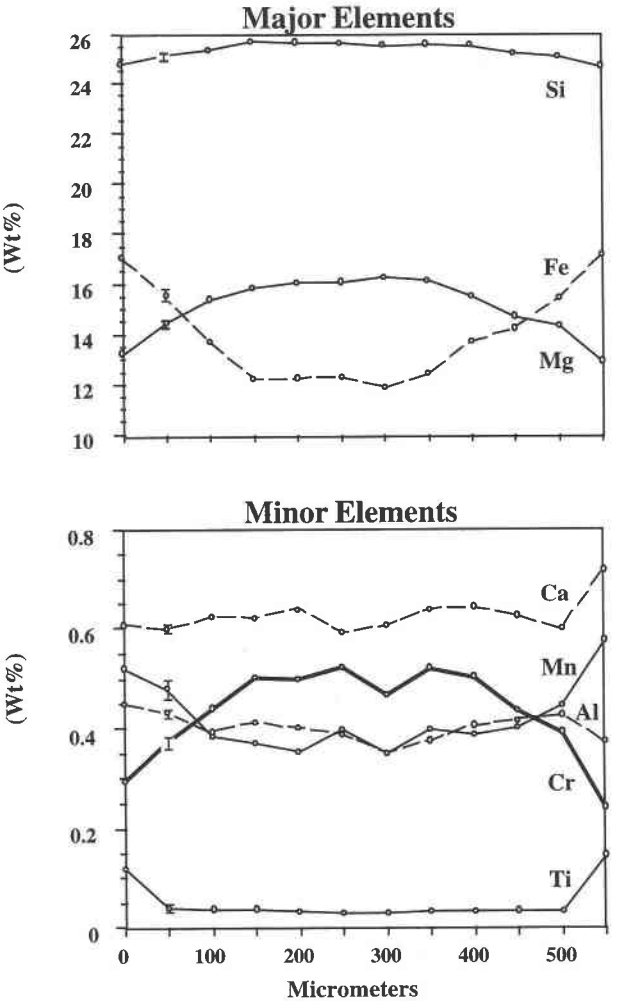

Figure 2. Electron microprobe traverse across a compositionally zoned Garland orthopyroxene. One sigma error bars are provided for some analytical points. After Fowler et al. (1994).

ment of a newer generation of ion microprobes, it is possible to analyze a large number of trace elements with great accuracy and precision using a microbeam technique.

The major thrust of this paper is the interpretation of selected trace elements (the REE, La, Ce, Nd, Sm, Eu, Dy, Er, Yb along with Y, Zr, and Sr) analyzed in the cores of orthopyroxene by secondary ion mass spectrometry (SIMS) techniques. Details of our analytical approach are given in Fowler et al. (1995) and Papike et al. (1995). The discussions presented here are based on approximately 2900 electron microprobe (EMP) and 365 SIMS analyses, all conducted in the electron microprobe and ion microprobe laboratories at the University of New Mexico. Our group has conducted SIMS studies of pyroxenes from a variety of planetary cumulates, including lunar norites (Papike et al. 1994a), martian orthopyroxenites (Papike et al. 1994b), asteroidal orthopyroxenites (diogenites, Fowler et al. 1994, 1995), asteroidal pyroxene-plagioclase cumulates (cumulate eucrites, Pun and Papike 1995), and terrestrial orthopyroxenites and norites (Stillwater Complex, Papike et al. 1995).

Potential problems with using pyroxene as a recorder of magmatic processes

Any process that alters the igneous signature resulting from mineral-melt partitioning greatly compromises the use of cumulus minerals as recorders of melt characteristics. Several studies have documented evidence of postcrystallization reequilibration on a variety of planetary cumulates. Phinney et al. (1993) used a microdrilling technique that removed 40–100 μm diameter cores from mineral grains in thin sections to sample pyroxene and plagioclase in eucrites. Samples obtained from this microdrilling technique were subsequently analyzed by INAA techniques. These investigators found strong evidence for REE, Fe, and Mg redistribution among pyroxene, plagioclase, and mesostasis. Schnetzler and Philpotts (1969) conducted isotope dilution studies of pyroxene and plagioclase separates from the Moore County cumulate eucrite. They concluded that the chondrite-normalized REE patterns of plagioclase and pyroxene indicate subsolidus trace element redistribution. Fowler et al. (1994, 1995) found chemically zoned orthopyroxene grains (Figs. 2 and 3) in the Garland diogenite. Because most diogenites are breccias and the cumulus orthopyroxene grains

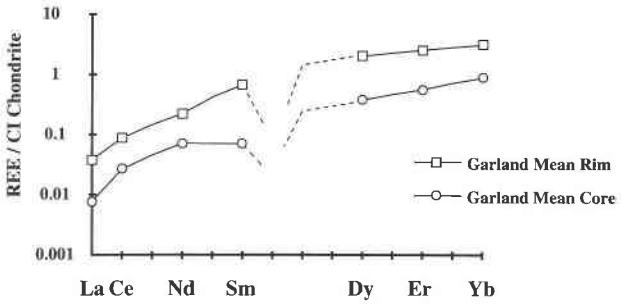

FIGURE 3. Mean rim and core REE patterns for a zoned orthopyroxene found in Garland. Eu values were below detection. These patterns have negative Eu anomalies as indicated by dashed lines. All REE patterns were normalized to CI chondrite (Anders and Grevesse 1989). After Fowler et al. (1995).

are fractured, analyses of different fragments would lead to a wide range of predicted melt compositions. Fowler et al. (1995) minimized this potential interpretive problem by using the lowest values of the incompatible trace elements as the best approximation of cumulus grain-core compositions.

For most of our studies, we analyzed primary orthopyroxene cumulus grains. The pattern of augite exsolution from these grains is usually straightforward with augite lamellae oriented on the host orthopyroxene (100) planes. If the augite lamellae are relatively thin (~1–2 μm) they can be easily reintegrated by either EMP or SIMS analyses using a rather broad beam. However, in our studies of cumulus orthopyroxene grains from the Stillwater Complex (Papike et al. 1995) we noted that thin rims (tens of micrometers) around the grains were free of visible (100) augite lamellae, but discrete augite grains rimmed these crystals. The interpretation of this texture (Fig. 4) is that the augite component diffused out of the host orthopyroxene and nucleated at grain boundaries to form discrete grains of augite. We found that these augite-free rims are depleted in certain incompatible trace elements relative to the cores of the grains (Fig. 5). However, because the rims are thin, most of the volume of the cumulus orthopyroxene grains appears uncompromised.

We avoided analyzing cumulus pigeonite grains for most of our investigations because when pigeonite inverts to orthopyroxene by slow cooling, a very complex exsolution texture results. The inverted pigeonite texture is observed as augite lamellae oriented on the monoclinic pi-

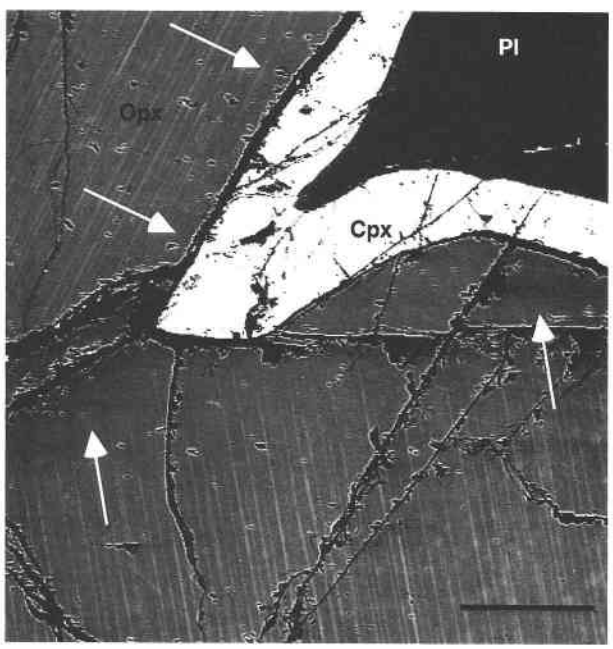

FIGURE 4. Backscattered electron (BSE) images showing examples of lamella-free zones at the rims of orthopyroxene (Opx), shown in medium gray. Clinopyroxene (Cpx) is white and plagioclase (Pl) is dark gray. Fine lamellae on the (100) planes of orthopyroxene are visible in both crystals but stop short of the crystal rims, indicated by the arrows. Scale bar is 100 μm. After Papike et al. (1995).

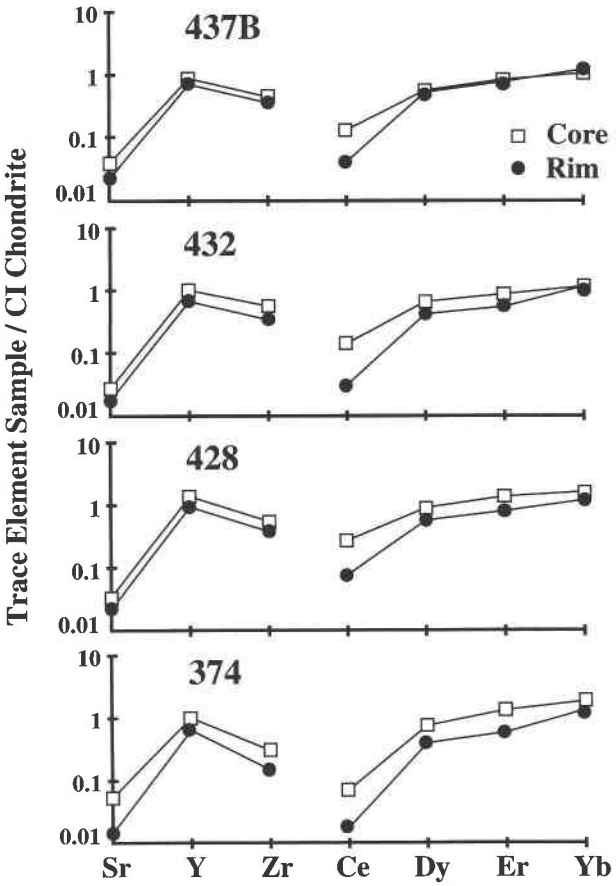

FIGURE 5. Core and rim orthopyroxene analyses of four samples from the Mountain View (Stillwater Complex) sample suite. The rims, which are free of optically visible augite exsolution lamellae, have significantly lower Ce and slightly lower Sr, Y, Zr, Dy, Er, and Yb than the cores. After Papike et al. (1995).

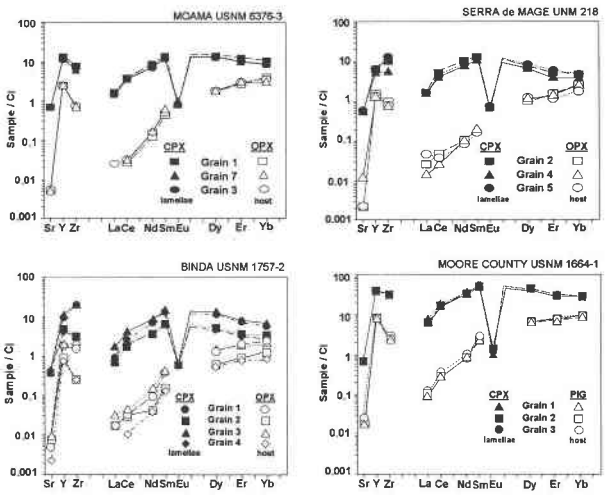

FIGURE 6. Chondrite-normalized trace element patterns of high- and low-Ca pyroxene lamellae and host pairs. Gd was estimated. After Pun and Papike (1995).

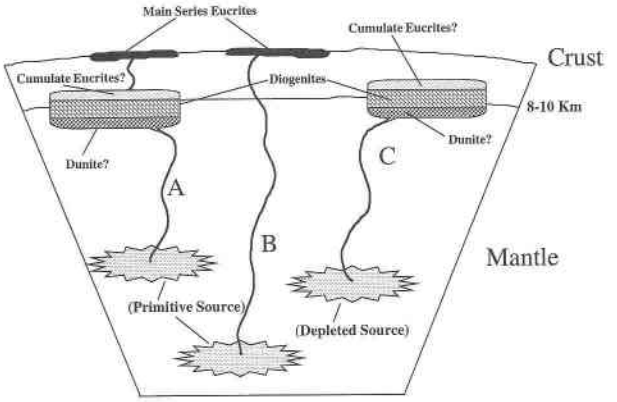

FIGURE 7. Schematic cross section of 4 Vesta showing aspects of different models that have been proposed to explain the petrologic relationship between main group eucrites, diogenites, and cumulate eucrites. After Fowler et al. (1995).

geonite (001) planes (formed before inversion), augite lamellae oriented on the orthopyroxene (100) planes (formed after inversion), and "wormy" augite blebs indicative of diffusional processes leading toward augite-orthopyroxene phase separation.

Redistribution of REE, Sr, Y, and Zr between augite and orthopyroxene can be very significant (Pun and Papike 1995). Figure 6 illustrates partitioning of incompatible trace elements between augite and orthopyroxene or augite and pigeonite from inverted pigeonite in several cumulate eucrites. Table 1 presents selected low-Ca pyroxene-augite partition coefficients determined by Pun and Papike (1995). The REE partitioning behavior reflects the different pyroxene crystal structures. The structures can rationalize the trace element patterns and abundances illustrated in Figure 6. The three relevant pyroxene space groups are $C2/c$ for augite, $P2_1/c$ for pigeonite, and $Pbca$ for orthopyroxene. All the pyroxene structures contain alternating tetrahedral and octahedral layers parallel to the (100) plane. The tetrahedral layer consists of infinite chains of corner-sharing tetrahedra that run parallel to the c axis. The octahedral layer is distorted and is composed of sixfold–eightfold-coordinated M2 sites and octahedral M1 sites. The M1 octahedra share edges to form infinite chains that run parallel to the c axis. In clinopyroxene the M2 polyhedra can be either sixfold or eightfold coordinated depending on their site occupancy. When the M2 site is occupied by Ca^{2+} or Na^{+} it has eightfold coordination; when occupied by smaller ions such as Mn^{2+}, Fe^{2+}, Mg^{2+}, and Li^{+}, the site becomes sixfold coordinated. Cameron and Papike (1981) showed that in orthopyroxene the M2 site is constrained in size as a direct result of the octahedral stacking sequence and therefore cannot easily accommodate ions larger than Mn^{2+}. On the other hand, the stacking sequences in augite and pigeonite allow a great deal of flexibility of the M2 site, which can then accommodate either larger ions such as Ca^{2+} and Na^{+} in eightfold coordination or smaller ions such as Mg^{2+} in sixfold coordination. The REEs in pyroxenes are largely restricted to the M2 site because the M1 site does not have the flexibility to expand to accommodate them. As shown by Shearer et al. (1989), there is an enrichment of REE abundances in high-Ca pyroxenes over those in low-Ca pyroxenes because of the larger M2 site of the augite structures. The Ca ions found within the augite structures have been experimentally and quantitatively shown to "prop" open the M2 site and, thus, increase the REE abundances (McKay 1989). The different octrahedral stacking sequences place a tight constraint on the size of the M2 site in orthopyroxene, excluding the LREEs and, therefore, producing the steep slopes seen in the patterns. The HREEs are more readily incorporated in the low-Ca pyroxenes because of their smaller ionic radii and consequently have shallower slopes than LREEs. The other trace elements, Sr, Y, and Zr, behave similarly in pyroxene among the cumulate eucrites (Fig. 6). These elements are more depleted in the low-Ca pyroxenes than in the high-Ca pyroxenes, reflecting analogous crystal-chemical constraints on their behavior as the REEs. Sr

TABLE 1. Trace element solid-solid partition coefficients D (low-Ca/Aug) between high-Ca and low-Ca pyroxene in cumulate eucrites

Element	Binda	Moama	Serra de Magé	Moore County
Sr	0.014	0.008	0.010	0.029
Y	0.181	0.209	0.228	0.211
Zr	0.090	0.105	0.087	0.081
La	0.014	0.010	0.018	0.016
Ce	0.010	0.008	0.008	0.019
Nd	0.011	0.020	0.011	0.027
Sm	0.026	0.042	0.023	0.050
Dy	0.113	0.138	0.150	0.150
Er	0.241	0.280	0.273	0.258
Yb	0.346	0.387	0.513	0.334

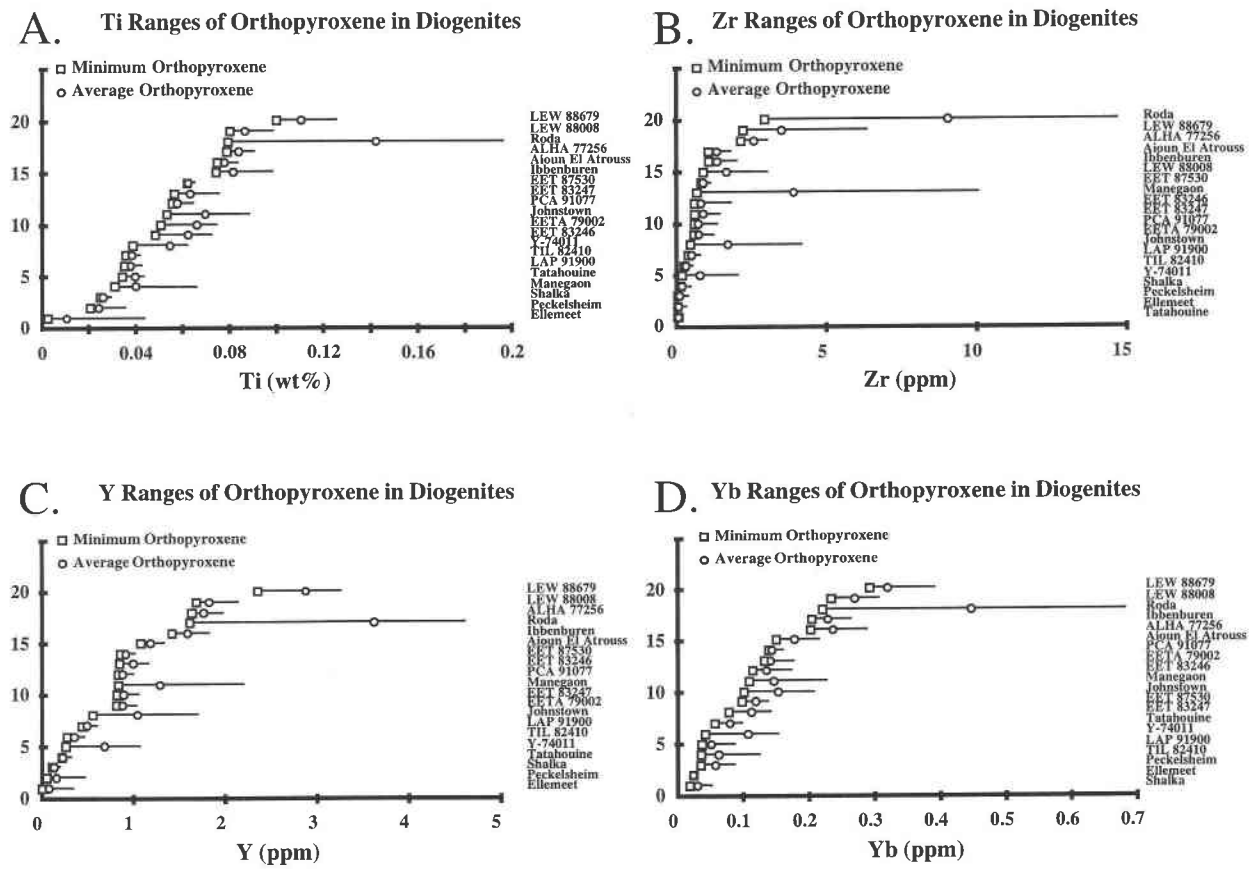

FIGURE 8. Diagrams showing minimum, average, and range of (A) Ti, (B) Zr, (C) Y, and (D) Yb for diogenites analyzed by SIMS. The minimum values may be the best approximation of the orthopyroxene core concentrations. After Fowler et al. (1995).

systematically follows Ca, reflecting the geochemical similarity of the two elements. Y is similar to the heavy REEs, and is more compatible than the light REEs. Zr generally follows Y, although there is some variability in the Zr concentrations.

Thus, it is clear that augite exsolution from either cumulus orthopyroxene or pigeonite greatly fractionates REE, Sr, Y, and Zr, and any process that separates the augite exsolution lamellae from the host cumulus grain greatly compromises the "igneous" trace element signature.

ASTEROIDAL CASE HISTORY

There are now four planetary bodies for which we have identified sample suites: Earth, Mars, Moon, and asteroid 4 Vesta. A suite of meteorites referred to as HED (howardites, eucrites, diogenites) has been linked to 4 Vesta (Consolmagno and Drake 1977; Drake 1979; Binzel and Xu 1993). Eucrites are pigeonite-plagioclase basalts and diogenites are orthopyroxenites. As a first approximation, howardites are two-component brecciated mixtures of eucrites and diogenites. Recent work by Zellner et al. (1995) shows images of Vesta taken with the planetary camera of the Hubble Space Telescope. Hubble's images provide the best view yet of Vesta's complex surface showing geologic complexity similar to the other terrestrial planets. Though only 525 km in diameter, Vesta has had a complex history, with basalts (eucrites) forming a significant part of its crust and with lower crust-mantle assemblages of orthopyroxenite (diogenites) and possibly dunite (olivine has been identified in spectral imaging, but no samples have yet been recovered). Eucrite, howardite, and diogenite members of the achondrite meteorites are considered to be genetically related (Mason 1962; Stolper 1977; Takeda et al. 1979; Bartels and Grove 1991; Grove and Bartels 1992). However, the nature of the relationships have long been debated. The relationship between eucrites and diogenites can be viewed within the context of two distinctly different models: (1) fractional crystallization and (2) partial melting. In fractional crystallization models (Mason 1962; Warren 1985; Warren and Jerde 1987; Bartels and Grove 1991; Grove and Bartels 1992), eucrites and diogenites represent a complementary continuum of planetary fractional crystallization products in which diogenites represent crystal accumulation during the crystallization of primary magmas at shallow to deep levels in the eucrite parent body (EPB), and eucrites represent residual melts. Alternatively, experimental studies may be interpreted to indicate that eucrites represent partial melts of a primitive, chondritic

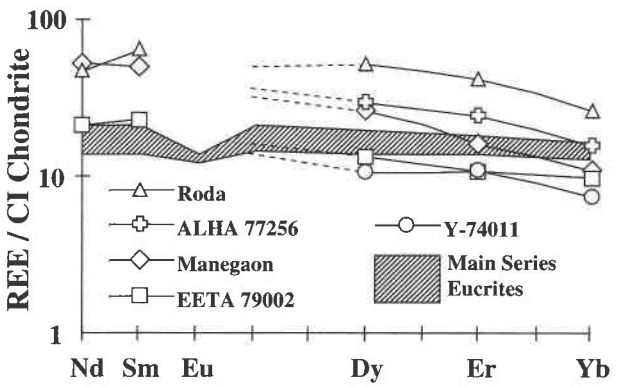

FIGURE 9. Estimated REE abundances of diogenite parental magmas and a field of main group eucrites defined by Stannern and Pasamonte. Some calculated LREE abundances for the diogenitic magmas were omitted because of their extremely low concentrations in the orthopyroxene. After Fowler et al. (1995).

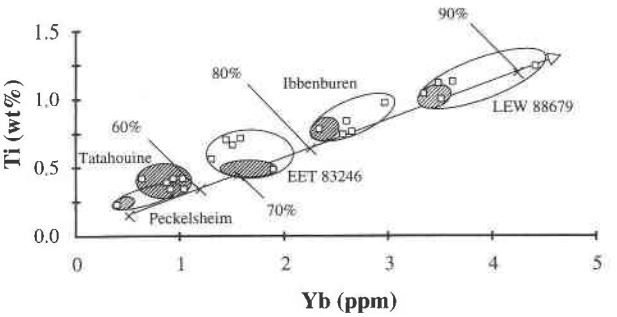

FIGURE 11. Estimated melt compositions for model 1 from orthopyroxene in selected diogenites are plotted in terms of Ti vs. Yb. A field of estimated melts for each diogenite is shown with a shaded region that may represent the melt composition during the crystallization of orthopyroxene cores. A fractional crystallization trajectory that passes through these diogenites is plotted. Estimated melts and the trajectory of fractional crystallization were calculated assuming constant D_i. After Fowler et al. (1995).

EPB mantle (Stolper 1977; Consolmagno and Drake 1977). Within this type of model, diogenites are still generally considered to be cumulates, but their petrogenetic relationship to the eucrites is less clear. In any case, diogenites can be considered as orthopyroxene cumulates in mafic intrusions from asteroid 4 Vesta. A schematic cross section of Vesta showing aspects of the different petrogenetic models that have been proposed is presented in Figure 7.

We have studied orthopyroxene from diogenites using both EMP (Fowler et al. 1994) and SIMS (Fowler et al. 1995) to provide more insight into their origin. The incompatible minor (Ti) and trace (Yb, Y, Zr) elements show a wide range of concentrations and suggest that the diogenites might be related by a fractionation sequence (Fig. 8).

If the diogenites and eucrites are petrogenetically related by a single or series of fractional crystallization events, then this should be supported by the trace element systematics of these respective magmas. Using the partition coefficients given in Fowler et al. (1995) and orthopyroxene trace element core compositions, the incompatible trace element characteristics were calculated for diogenitic parental melts. The calculated REE melt compositions, parental to diogenites, are shown in Figure 9 along with a field showing the main group eucrites. Figure 10 compares Ti and Yb for the calculated diogenitic parental melts and main group eucrites. Figures 9 and 10 indicate that the estimated diogenite melt compositions show a broader range in composition than the eucrite trend. Therefore, it seems unlikely that the eucrites are residual melts derived from the fractional crystallization of a magma that produced the diogenites. Instead, the comparison between the calculated diogenitic melts and bulk eucrite compositions suggests that the diogenites represent orthopyroxene cumulates from magmas unrelated by crystallization processes to the eucrites.

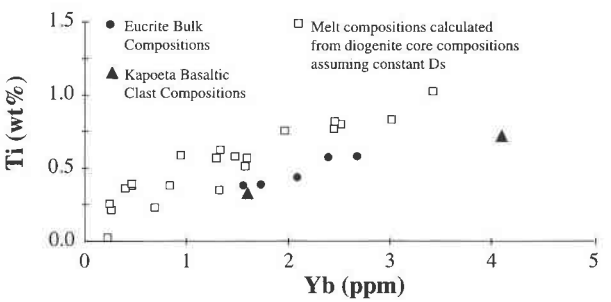

FIGURE 10. Plot of Ti vs. Yb showing a trend formed by calculated diogenite melt compositions and a field containing eucritic compositions, including the main group eucrites defined by Stannern and Pasamonte, and Kapoeta basaltic clast compositions. After Fowler et al. (1995).

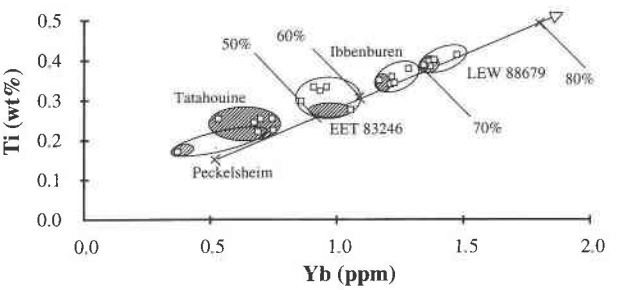

FIGURE 12. Estimated melt compositions for model 2 from orthopyroxene in diogenites are plotted in terms of Ti vs. Yb. A field of estimated melts for each diogenite is shown with a shaded region that may represent the melt composition during the crystallization of orthopyroxene cores. A fractional crystallization trajectory that passes through these diogenites is plotted. Estimated melts and the trajectory of fractional crystallization were calculated assuming a factor of three variation in D over the interval of crystallization. After Fowler et al. (1995).

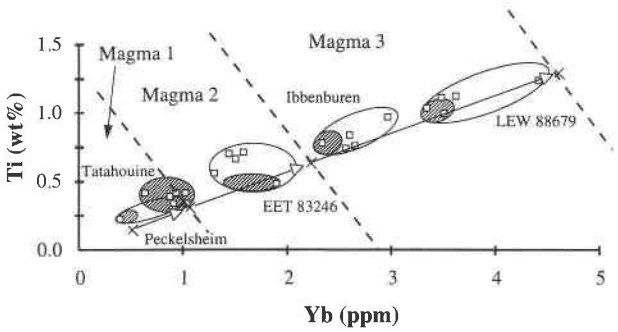

FIGURE 13. Estimated melt compositions for model 3 from orthopyroxene in diogenites are plotted in terms of Ti vs. Yb. Three intervals of 55% fractional crystallization defining three possible reservoirs of magma are indicated by dashed lines. A field of estimated melts for each diogenite is shown with a shaded region that may represent the melt composition during the crystallization of orthopyroxene cores. A fractional crystallization trajectory that passes through these diogenites is plotted. Calculations assumed constant D for the intervals of crystallization. After Fowler et al. (1995).

In our previous study (Fowler et al. 1995), we considered three models describing possible crystallization scenarios for diogenite parental melts. Model 1 (Fig. 11) considers all the diogenites to be related to a single melt reservoir and assumes that Ds do not vary with crystallization. Model 2 (Fig. 12) is identical to model 1 except the Ds used in the modeling increase by a factor of 3. Model 3 (Fig. 13) considers that there were several reservoirs involved in the crystallization of diogenites. However, the problem with all these models is that they predict a high percentage of fractional crystallization (model 1, >90%; model 2, >70%; model 3, >55%) for each magma. It appears highly unlikely that with this amount of crystallization a basaltic magma would not crystallize plagioclase. However, diogenites contain extremely low abundances of plagioclase. A possible way around this problem is to assume that the magmas parental to the diogenites may have been unusual, essentially hypersthene normative basalts. This model was proposed earlier by Stolper (1977), Mittlefehldt (1994), and Jurewicz et al. (1995). A basaltic melt with higher normative hypersthene would result in more extreme orthopyroxene crystallization and a greater change in temperature and melt composition over which the orthopyroxene crystallized. This would result in a more extensive orthopyroxene lithology in layered intrusions. In summary, the results of our previous studies (Fowler et al. 1994, 1995) indicate that the diogenites are not related to the eucrites

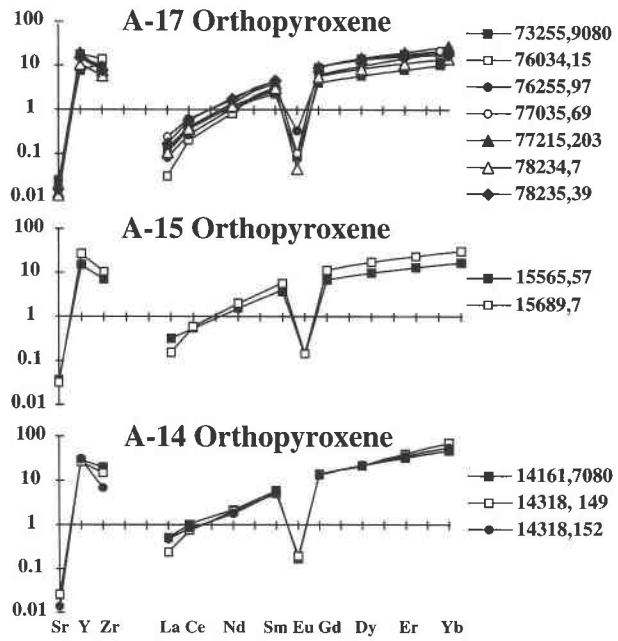

FIGURE 14. Average normalized trace element patterns for orthopyroxene and estimated patterns for parental melts. After Papike et al. (1994a).

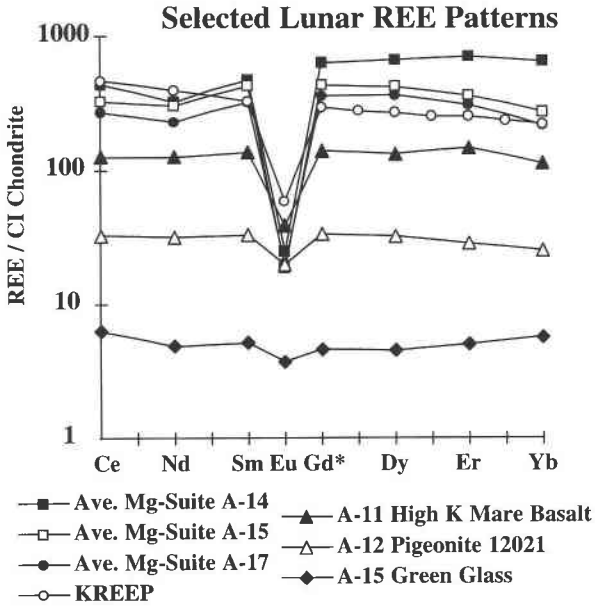

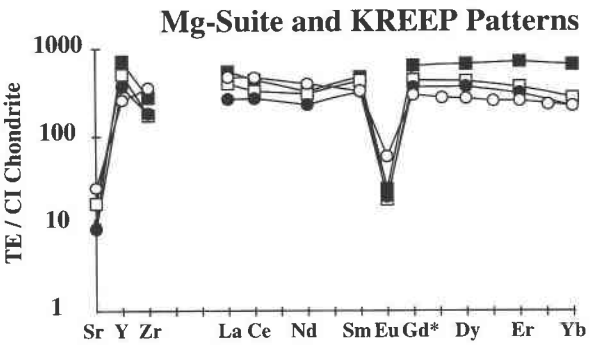

FIGURE 15. Estimated trace element patterns for melts parental to Mg-suite norites compared with other lunar rock types. After Papike et al. (1994a).

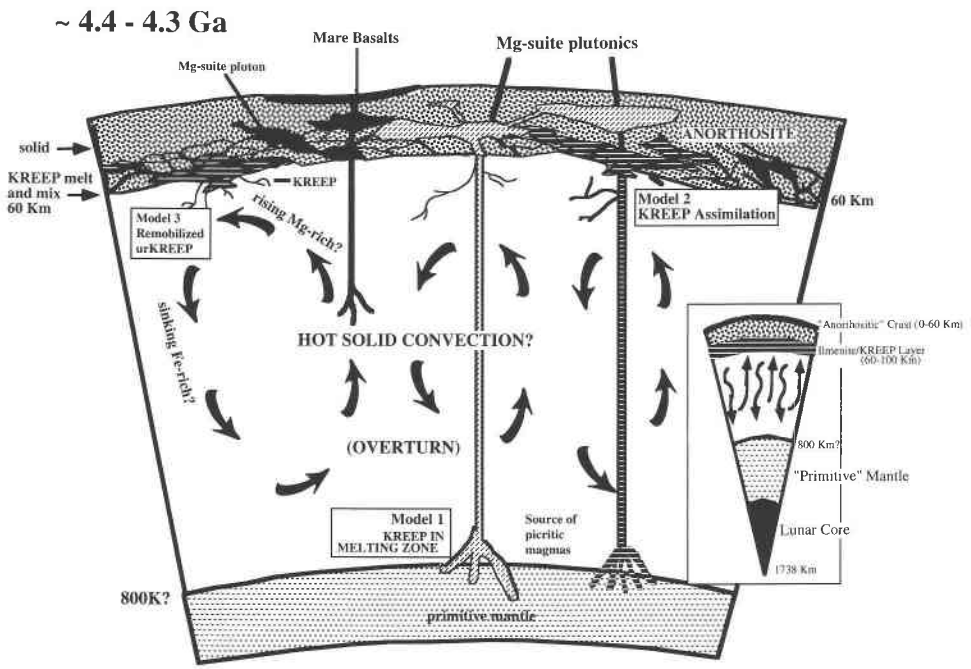

FIGURE 16. Schematic cross section of the Moon showing possible petrogenetic models for the origin of the Mg-suite rocks. Modified from a diagram provided by Graham Ryder (1994, personal communication).

by crystallization processes and that they are derived from a mantle source different from the eucritic magmas or one that was already depleted because of earlier eucrite extraction.

LUNAR CASE HISTORY

Shortly after the first lunar rocks were returned to Earth in 1969, an extremely important discovery involved the realization that the early history of the Moon could have been dominated by a global magma ocean. Although this hypothesis has never been proved, it remains the leading model for the early differentiation of the Moon. One recent interpretation (Hess and Parmentier 1995) of the global consequences of a lunar magma ocean with a depth of 800 km is that plagioclase could have floated, forming a 60 km anorthositic crust near the lunar surface. The denser olivine and pyroxene probably sank, forming a cumulate pile ~700 km thick with the denser Fe-rich pyroxene assemblages near the top and less dense, more magnesian, olivine, and pyroxene assemblages near the bottom. Hess and Parmentier (1995) suggested that late-crystallizing melt was rich in trace incompatible elements forming a KREEP (K, rare earth elements, and P) residue that was also rich in ilmenite. If this model is correct, it leads to a gravitationally unstable cumulate pile, with dense cumulates overlying less dense cumulates. The predicted consequence of this instability (Spera 1992; Hess and Parmentier 1995) is convective overturn with the ilmenite layer (which also contains KREEP and heat-producing elements) sinking to deep mantle depths. Although this model is speculative, it potentially explains how KREEP, a late-crystallizing product of the magma ocean, can be brought to great depth in a zone of melting, which may include both Mg-rich cumulates and primitive mantle. This process could provide source regions for the picritic lunar basalts (Shearer and Papike 1993) and Mg- and Al-rich magmas (the Mg suite), which intruded the anorthositic crust during the period 4.43–4.1 Ga after most of the magma ocean had crystallized (Taylor et al. 1993; Warren and Kallemeyn 1993). This discussion focuses on the petrogenesis of the Mg-suite magmas (Papike et al. 1994a), which apparently intruded the

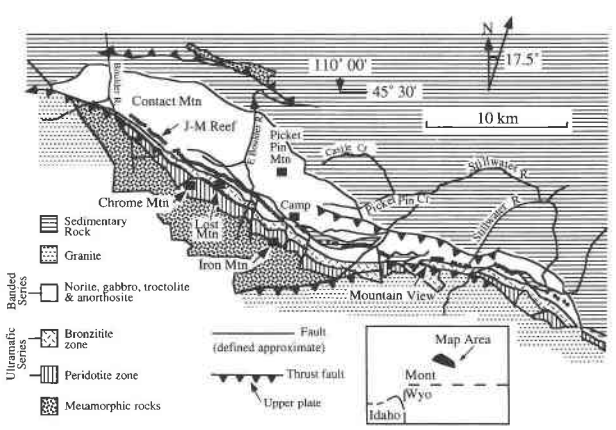

FIGURE 17. Generalized geologic map of the Stillwater Complex, Montana (after Lambert and Simmons 1987).

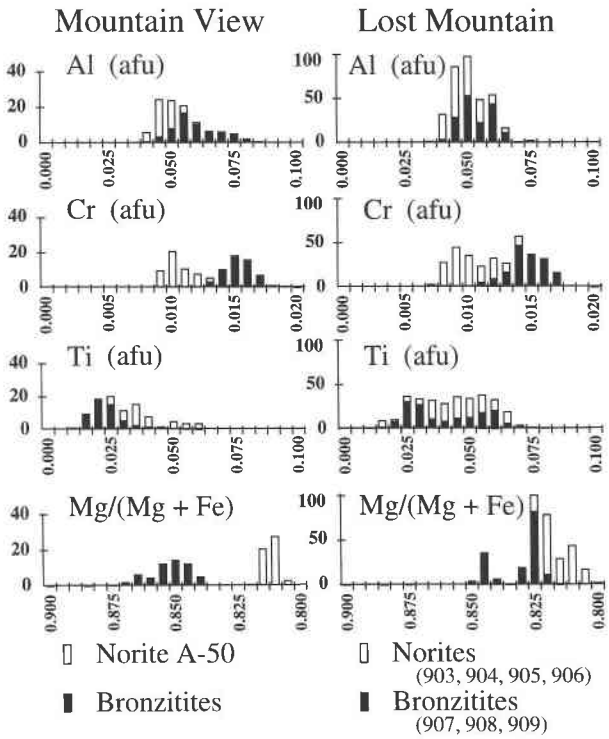

FIGURE 18. Histograms of EMP data for Mountain View and Lost Mountain sample suites. Open bars represent norites and solid bars represent bronzitites. Afu = atoms per formula unit. After Papike et al. (1995).

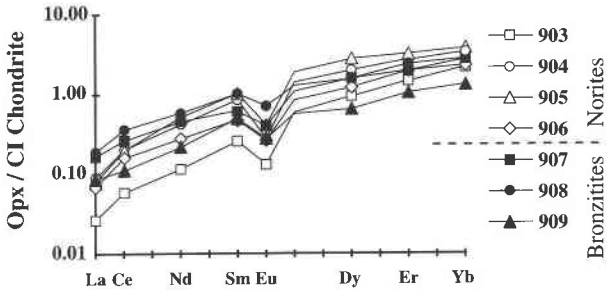

FIGURE 19. Chondrite-normalized REE for orthopyroxene from the Lost Mountain sample suite. REEs are normalized to the chondrite data of Anders and Grevesse (1989). After Papike et al. (1995).

anorthositic crust and may have formed layered mafic complexes (James 1980) similar to the Stillwater Complex, Montana.

Many of the samples representing the Mg suite are small and thus unrepresentative. In addition, they are cumulates and thus are difficult to study using whole-rock analytical techniques. Therefore, we used SIMS techniques to analyze a suite of trace elements in cumulus orthopyroxene from Mg-suite norites. The 12 norite samples investigated by Papike et al. (1994a) were selected from a compilation by Warren (1993), who attempted to select the best candidates from the standpoint of their pristine character, i.e., those samples not formed or contaminated by impact processes. Figure 14 illustrates our chondrite-normalized (Anders and Grevesse 1989) REE, Sr, Y, and Zr data for orthopyroxene in our 12 noritic samples. Only averages are plotted from the ~50 SIMS analyses of the 12 samples. See Papike et al. (1994a) for a discussion of the *D*s used to estimate melt compositions. The REE contents of the orthopyroxene are high and relatively uniform, reflecting the very high REE concentrations of their parental melts. The uniform nature of the REE, Y, and Zr concentrations in these pyroxenes strongly suggests that the concentrations were inherited from their parental melts and were not the result of some fictive metasomatic fluid that added the trace elements to these noritic rock types after crystallization (e.g., Snyder et al. 1994). Figure 15 compares normalized trace element concentrations for estimated average Apollo 14, 15, and 17 melts that were parental to noritic rock types with several other lunar rocks. The KREEP estimate is from Warren (1989) for his average high-K KREEP. The estimated REE contents for A-14, A-15, and A-17 melts are extremely high, especially for the heavy REEs. Therefore, no simple process of mixing a high-K KREEP with a picritic melt can produce the enriched patterns that we estimated. Apparently, advanced fractionation of the Mg-suite plutons, and especially plagioclase crystallization, superimposed on the addition of KREEP, must have contributed to the extreme HREE enrichments. The KREEP component could have been added either to an Mg-rich (picritic?) melt deep in the Moon (model 1, Fig. 16, e.g., Shearer and Papike 1993) or by the assimilation of KREEP (model 2, Fig. 16) at much shallower levels (60–100 km) below the anorthositic crust. The sinking KREEP-rich cumulates (Hess and Parmentier 1995) could have had three to ten times the heat-producing elements contained in the bulk Moon and thus potentially provide the heat source for deep melting. Model 3 is a scenario by which Ur KREEP (KREEP that represents the last dregs of crystallization from the magma ocean) is remobilized, possibly by decompressional melting caused by impact.

Snyder et al. (1995a, 1995b) pursued these ideas of KREEPy magmas being parental to Mg-suite lithologies. To test this hypothesis, they compiled compositions of relatively primitive and pristine KREEP basalts from the Apollo 15 landing site. These authors did not address the ultimate origin of the KREEPy parental magmas but assumed that they were products of deep melting in the lunar interior, which subsequently assimilated KREEPy residual liquids (from the magma ocean) during passage of the basalt to the lunar surface. Snyder et al. (1995a, 1995b) modeled fractional crystallization using an average KREEP magma under 1 bar. This fractionation sequence was then used to calculate mineral compositions and trace element compositions of successive liquids. The trace element compositions of these successive KREEP-basalt residual liquids were compared with liquid compositions calculated from trace element data from ortho-

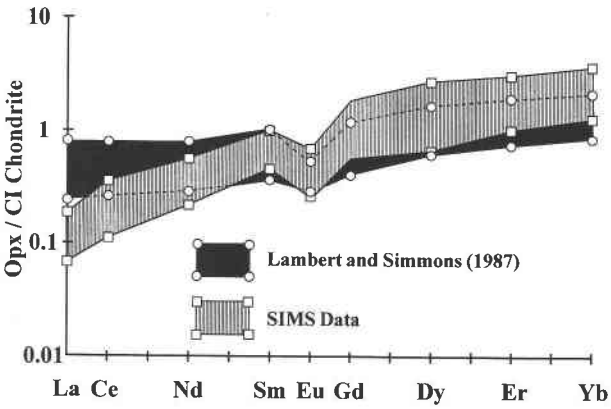

FIGURE 20. Comparison of ranges of chondrite-normalized REE determined by isotope dilution (Lambert and Simmons 1987) and SIMS (Papike et al. 1995) for orthopyroxene from Lost Mountain. After Papike et al. (1995).

pyroxene (Papike et al. 1994a). The calculated KREEP-basalt residual liquids are within the range of parental liquids calculated using the data of Papike et al. (1994a), lending additional support to KREEPy parental magmas for lunar Mg-suite lithologies.

TERRESTRIAL CASE HISTORY: THE STILLWATER COMPLEX, MONTANA

Because our planetary samples of orthopyroxenites (e.g., diogenites from 4 Vesta and a single sample from Mars, ALH 84001, discussed below) and norites (lunar Mg suite) are usually small brecciated samples that lack a good geologic field context, we looked to a well-studied terrestrial occurrence that had orthopyroxenite lithologies. We selected the Bronzitite zone of the Ultramafic series of the Stillwater Complex, Montana, because it has several similarities to diogenites, and because it is arguably the best-studied terrestrial occurrence of an orthopyroxenite sequence.

A comprehensive review of previous work on the Stillwater Complex is provided in Czamanske and Zientek (1985). The Stillwater Complex, located in southwestern Montana, strikes northwest-southeast, approximately parallel to the north margin of the Beartooth Mountains, and dips steeply to the north (Fig. 17). The age of the complex is 2701 ± 8 Ma (DePaolo and Wasserburg 1979). The complex is divided into a Basal series, an Ultramafic series, and a Banded series. The boundary between the Basal series and the Ultramafic series is marked by the appearance of cumulus olivine, whereas the lowest boundary of the Banded series is defined as the horizon where plagioclase first appears as a cumulus phase. The Ultramafic series is subdivided into a lower Peridotite zone in which olivine or olivine + orthopyroxene are the cumulus minerals and an upper Bronzitite zone in which orthopyroxene is the only cumulus mineral. Orthopyroxene in the entire Bronzitite zone is remarkably constant

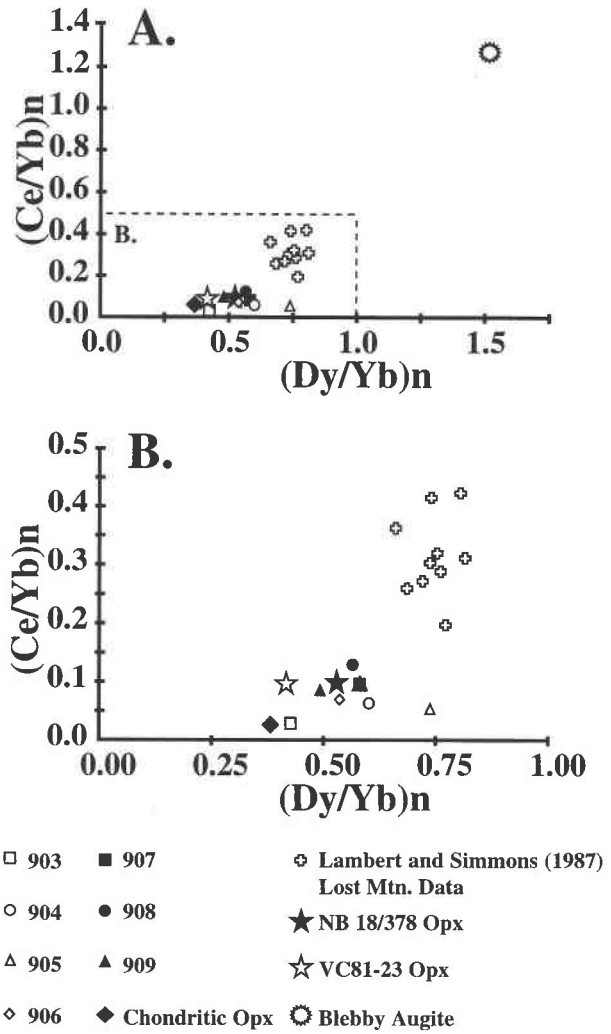

FIGURE 21. Orthopyroxene $(Ce/Yb)_n$ vs. $(Dy/Yb)_n$ systematics. Isotope dilution data (Lambert and Simmons 1987) and SIMS data (Papike et al. 1995) are compared. Estimated $(Ce/Yb)_n$ and $(Dy/Yb)_n$ for orthopyroxene that would crystallize from Stillwater sills NB 18/378 and VC 81-23 are also plotted. Orthopyroxene crystallizing from a chondritic melt (Anders and Grevesse 1989) is shown for reference. (**A**) Augite plots in the upper right corner. The result of intercumulus augite contamination of cumulus orthopyroxene mineral separates would cause analytical results to plot on a mixing line between the group of orthopyroxene and the augite. **B** is a magnified view of the lower left portion of **A**. After Papike et al. (1995).

in composition, with the atomic ratio Mg/(Mg + Fe) = 85 ± 1 (Raedeke and McCallum 1984). Raedeke and McCallum concluded that simple fractional crystallization with crystal settling is not sufficient to explain the lithologic sequences observed in the Ultramafic series. They proposed a model in which accretion of cumulates and growth of the magma chamber proceeded through periodic influxes of olivine-saturated basaltic magma that initially pooled on or near the magma chamber floor. Fe-

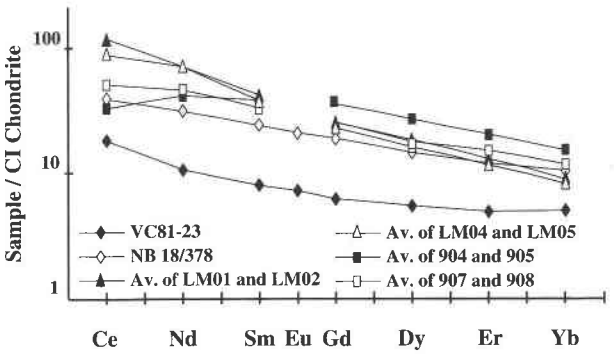

FIGURE 22. Melt REE patterns calculated from orthopyroxene REE determined by isotope dilution and SIMS. Norite samples LM01 and LM02 and bronzitite samples LM04 and LM05 are from Lambert and Simmons (1987), determined by isotope dilution. Data on norite samples 904 and 905 and bronzitite samples 907 and 908 were determined by SIMS. Sills VC 81 and NB 18, which may represent parental melts, are included for comparison (REE data from Lambert and Simmons 1988). After Papike et al. (1995).

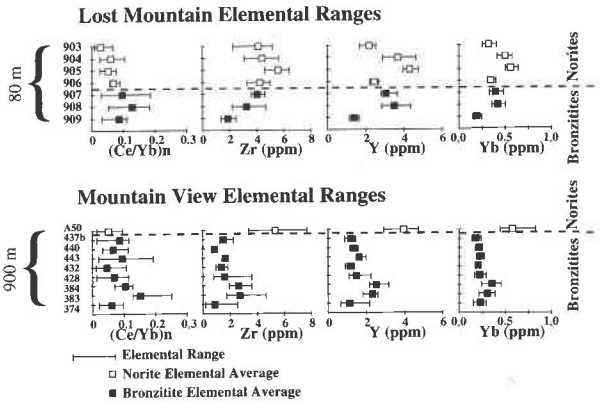

FIGURE 23. Selected trace element data for the Lost Mountain and Mountain View sample suites plotted with respect to stratigraphic position. The Lost Mountain suite spans 80 m, whereas the Mountain View suite spans 900 m. After Papike et al. (1995).

enrichment trends that would result from fractionation were suppressed by the effects of repeated injections of new magma, extrusion of fractionated magma, periodic equilibrium crystallization, and reaction of cumulates with trapped liquid.

Lambert and Simmons (1987) presented isotope dilution analyses of REE and microprobe analyses of 17 cumulus orthopyroxene separates from the Ultramafic series. They concluded that the Ultramafic series formed by multiple injection and fractional crystallization of magmas derived from the upper mantle by a dynamic melting process. These magmas were characterized by having rather high $(Ce/Yb)_n$ ratios of 8 to 18. Subscript n refers to the fact that elemental abundances were normalized to chondritic values (Anders and Grevesse 1989). Lambert and Simmons (1987) concluded that either the mantle source region was light-REE enriched or the partial melts were contaminated by light-REE–enriched crustal rocks.

The Bronzitite zone–Norite zone contact is of particular interest because it is the most prominent contact in the complex. It can be traced across the entire strike length and is marked by the abrupt appearance of cumulus plagioclase. However, this contact is not as simple as it appears at first glance. It has been interpreted as (1) the result of normal fractionation as the magma reached plagioclase saturation (Hess 1960), (2) the horizon at which suspended plagioclase began to accumulate on the floor of the chamber (McCallum et al. 1980), or (3) the product of an influx of a batch of plagioclase-saturated magma (Lambert 1982; Thurber and McCallum 1990). Raedeke (1982) compared the compositions of orthopyroxene grains on both sides of the contact and observed a decrease in Mg/(Mg + Fe) (~4 mol%), Cr_2O_3, and Al_2O_3 from the Bronzitite to the Norite zone.

Figure 18 is a series of histograms that illustrate some major and minor element differences between orthopyroxene compositions from the Norite and Bronzitite zones. It is clear that there are some significant differences in the orthopyroxene compositions, with orthopyroxene in the Norite zone having higher Ti and lower Cr, Al, and atomic Mg/(Mg + Fe). At least two models must be considered when explaining these systematics: (1) fractionation of a single magma that led to plagioclase saturation or (2) mixing of a second magma.

Figure 19 presents average (~5 SIMS analyses per grain) chondrite-normalized orthopyroxene REE plots for the Lost Mountain traverse. Although there are some differences between REE patterns from the Norite and Bronzitite zones, there is not a simple regular sequence from the stratigraphically lowest sample, 909, to the stratigraphically highest sample, 903. Sample 903 appears

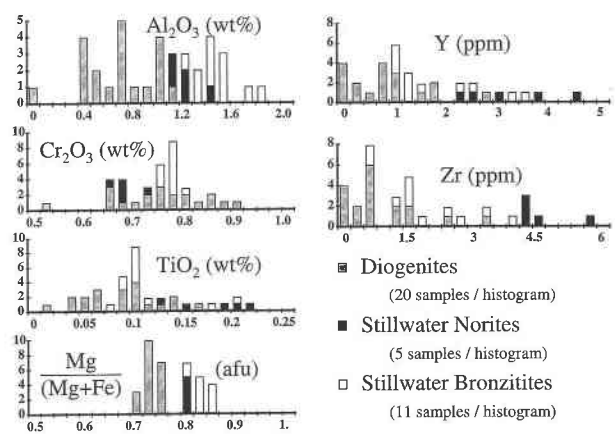

FIGURE 24. Histograms comparing the chemistries of orthopyroxene from diogenites and Stillwater bronzitites and norites. Atoms per formula unit = afu.

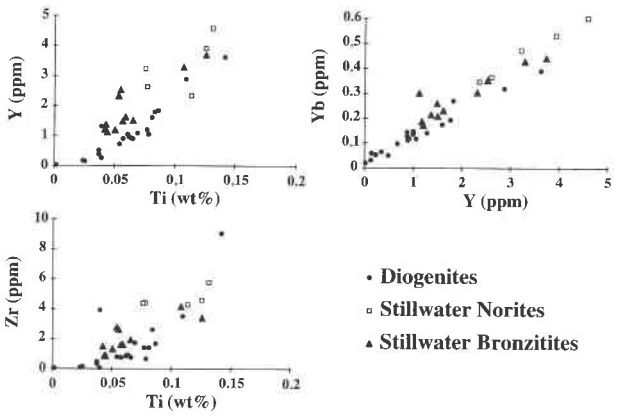

FIGURE 25. Incompatible-incompatible elemental plots for orthopyroxene from diogenites and Stillwater bronzitites and norites.

TABLE 2. Possible parental melt compositions for Stillwater Ultramafic series (Helz 1995) and diogenites (Bartels and Grove 1991)

	Mafic* norite 81VCZ-23	Mix* 50:50	Magnesian* gabbro-norite NB18/374	Kapoeta clast rho**
SiO_2 (wt%)	53.10	51.90	50.70	49.5
TiO_2	0.44	0.73	1.02	0.78
Al_2O_3	11.20	13.20	15.20	9.88
Σ FeO	14.70	12.72	10.74	18.8
MnO	0.18	0.18	0.18	0.54
MgO	12.70	11.02	9.33	10.10
CaO	7.00	8.50	10.00	9.34
Na_2O	0.41	1.11	1.83	0.47
Total	99.73	99.36	99.0	99.41
Mg/(Mg + Fe)*	0.61	0.61	0.61	0.49

* Calculated with total Fe as FeO; however, 10–20% may be Fe_2O_3.
** Analysis from Dymek et al. (1976).

anomalous because of its low REE content and lower LREE/HREE. This lack of simple systematics was also observed by Lambert and Simmons (1987). Nevertheless, the orthopyroxene REE patterns from the Norite zone generally show deeper negative Eu anomalies. It is apparent in comparing our SIMS results with the Lambert and Simmons isotope dilution data that their REE patterns for orthopyroxene show considerably higher LREE than we observed (Fig. 20). Figure 21 shows more clearly the differences between the SIMS data and isotope dilution data on a $(Ce/Yb)_n$ vs. $(Dy/Yb)_n$ diagram (Lambert et al. 1994). The isotope dilution data plot at significantly higher $(Ce/Yb)_n$ and $(Dy/Yb)_n$ than the SIMS data. In Figure 21 we plot an augite analysis to see what effect contaminating augite in a orthopyroxene mineral separate might have. The isotope dilution data plot on a mixing line between our SIMS orthopyroxene and augite points. Mass balance–mixing calculations indicate that approximately 5 wt% of augite added to the SIMS orthopyroxene REE analyses produces parallel patterns for the SIMS and isotope dilution data. Also plotted on Figure 21 are the "calculated orthopyroxene" compositions for two sills found beneath the Stillwater Complex that may represent parental melts of these Stillwater cumulates (Helz 1985; Lambert and Simmons 1988). One of them (sample NB 18/378) plots within the SIMS data cluster and the other (VC 81-23) plots near the cluster.

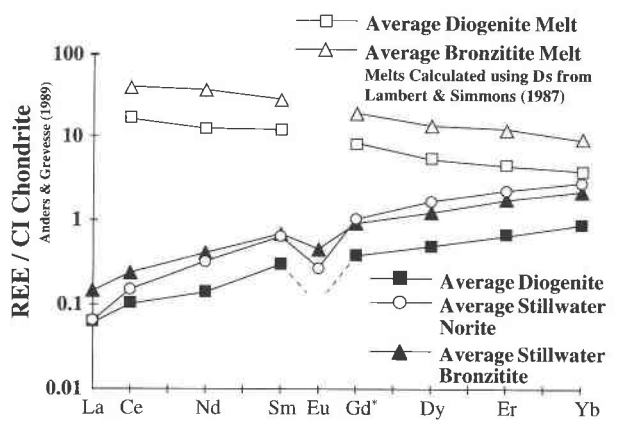

FIGURE 26. Average chondrite-normalized REE patterns (Anders and Grevesse 1989) for orthopyroxene from diogenites and Stillwater bronzitites and norites. Estimated REE patterns for melts parental to Stillwater bronzitite and diogenite are also illustrated. Eu was below detection limits for orthopyroxene from diogenite. Gd was estimated.

Figure 22 illustrates estimated REE melt compositions based on both the SIMS and isotope dilution data and the REE data for the two candidate parental-melt sills (Helz 1985). The data for the sills are from Lambert and Simmons (1988). The partition coefficients, from Lambert and Simmons (1987) are given in Papike et al. (1995). The differences between the isotope dilution and SIMS data for the orthopyroxene are reflected in the slopes of the calculated REE patterns. The Lambert and Simmons (1987) estimated melts (norite samples LM01 and LM02 and bronzitite samples LM04 and LM05) have higher LREE than those calculated from the SIMS data (norite samples 904 and 905 and bronzitite samples 907 and 908). The calculated melt for bronzitite samples 907 and 908 is quite similar to Mg-gabbronorite sill NB 18/378. It is apparent that melts calculated from orthopyroxene isotope dilution data have higher LREE than those calculated from the SIMS data.

Trace element systematics for the two sample suites are summarized in Figure 23. In examining this diagram we should take into account that the nine-sample suite from Mountain View spans ~900 m of stratigraphic section, whereas the seven-sample suite from Lost Mountain spans only 80 m across the Bronzitite-Norite zone contact. The $(Ce/Yb)_n$ values are presented as a slope index for the REE patterns. Although the variations with stratigraphic height are not systematic, average $(Ce/Yb)_n$ is lower in the Norite zone than in the Bronzitite zone. In the Moun-

TABLE 3. Average pyroxene major and minor element analyses by EMP

Sample	Low-Ti diog-enite	Inter-mediate Ti diog-enite	High-Ti diog-enite	Diog-enite	Still-water bronz-itite	Still-water norite	Cum. eucrite Moore Co.	Cumulate eucrites	Martian ALH 84001	Mg-suite A-14	Mg-suite A-15	Mg-suite A-17
SiO_2 (wt%)	55.1	54.4	54.3	54.6	55.5	55.1	51.6	52.7	54.2	54.0	54.0	54.4
Al_2O_3	0.5	0.7	1.0	0.7	1.5	1.2	0.3	0.5	0.7	0.9	1.5	1.0
TiO_2	0.05	0.09	0.14	0.09	0.12	0.18	0.35	0.22	0.14	0.70	0.41	0.44
Cr_2O_3	0.39	0.64	0.48	0.51	0.56	0.40	0.17	0.23	0.38	0.35	0.69	0.54
MgO	26.8	26.0	25.7	26.1	30.1	28.7	15.1	20.0	25.1	26.3	28.0	27.1
FeO	16.3	16.1	16.4	16.2	9.9	11.8	27.3	22.2	16.3	14.8	12.7	13.8
MnO	0.57	0.53	0.54	0.55	0.21	0.25	0.91	0.75	0.48	0.23	0.21	0.25
CaO	0.9	1.3	1.5	1.3	1.8	1.6	4.7	3.5	1.6	1.6	1.4	1.7
Na_2O	0.01	0.01	0.01	0.01	0.02	0.01	0.01	0.01	0.04	0.01	0.01	0.01
Total oxide	100.53	99.73	100.07	100.07	99.65	99.26	100.44	100.08	98.85	98.90	98.91	99.21
Si (afu)	1.984	1.977	1.972	1.978	1.962	1.972	1.990	1.983	1.989	1.968	1.950	1.969
$^{[4]}$Al	0.005	0.011	0.015	0.011	0.024	0.024	0.010	0.017	0.011	0.031	0.049	0.031
Total tetrahedral	1.989	1.989	1.987	1.988	1.986	1.996	2.000	2.000	2.000	1.999	1.999	2.000
$^{[6]}$Al (afu)	0.015	0.023	0.028	0.022	0.038	0.028	0.004	0.003	0.019	0.008	0.015	0.012
Ti	0.001	0.003	0.004	0.003	0.003	0.005	0.010	0.007	0.004	0.019	0.011	0.012
Cr	0.014	0.019	0.015	0.016	0.016	0.029	0.005	0.007	0.016	0.010	0.020	0.015
Mg	1.438	1.405	1.390	1.410	1.586	1.530	0.866	1.118	1.372	1.430	1.507	1.458
Fe	0.490	0.488	0.499	0.492	0.293	0.355	0.881	0.698	0.500	0.451	0.383	0.421
Mn	0.018	0.016	0.017	0.024	0.006	0.008	0.030	0.024	0.015	0.007	0.006	0.008
Ca	0.035	0.052	0.058	0.049	0.067	0.060	0.194	0.141	0.064	0.063	0.054	0.065
Na	0.000	0.001	0.001	0.000	0.002	0.001	0.001	0.000	0.003	0.001	0.001	0.000
Total M1 + M2	2.010	2.007	2.011	2.016	2.010	2.015	1.991	1.998	1.993	1.989	1.997	1.991
Mg/(Mg + Fe)	0.746	0.742	0.736	0.741	0.844	0.812	0.496	0.616	0.733	0.760	0.797	0.776
Wo	1.78	2.68	2.97	2.50	3.47	3.07	10.0	7.22	3.31	3.25	2.77	3.36
En	73.3	72.2	71.4	72.3	81.5	78.7	44.6	57.1	70.9	73.5	77.5	75.0
Fs	25.0	25.1	25.6	25.2	15.0	18.2	45.4	35.7	25.8	23.2	19.7	21.6

tain View traverse it is evident that sample A50 (norite) has significantly higher Zr, Y, and Yb than the samples from the Bronzitite zone. There is also some evidence of this in the Lost Mountain traverse but with much more scatter.

On the basis of the above discussion and other evidence summarized in Papike et al. (1995), the weight of evidence favors the introduction of a batch of plagioclase-saturated melt (± intratelluric plagioclase) at the top of the Bronzitite zone. REE concentrations in liquids calculated on the basis of orthopyroxene REE data are similar to REE abundances in magnesian gabbronoritic sills, lending support to Helz's (1985) conclusion that these sills would be suitable parental melts for the Ultramafic series.

Orthopyroxene from asteroid 4 Vesta and the Stillwater Complex, Montana

Comparative chemical data for orthopyroxene from diogenites and the Stillwater Complex are presented in Figures 24–26. For orthopyroxene from diogenites, it appears that the major element chemistry, especially Fe and Mg, may have been altered by crystal-melt interactions, subsolidus reactions, or both (Sack et al. 1991; Mittlefehldt 1994; Fowler et al. 1994). Nevertheless, the value of Mg′ [atomic ratio Mg/(Mg + Fe)] gives us some idea of the Mg′ of the parental melts. Although the Mg′ of orthopyroxene in diogenites shows a range from ~0.68 to ~0.82, the average Mg′ clusters near 0.74. Orthopyroxene from Stillwater bronzitite has Mg′ near 0.84 and

TABLE 4. Average pyroxene trace element analyses by SIMS

Sample	Low-Ti diog-enite	Inter-mediate-Ti diog-enite	High-Ti diog-enite	Diog-enite	Still-water bronz-itite	Still-water norite	Cum. eucrite Moore Co.	Cumulate eucrites	Martian ALH 84001	Mg-suite A-14	Mg-suite A-15	Mg-suite A-17
Sr (ppm)	0.120	0.167	0.211	0.164	0.240	0.187	0.806	0.658	0.126	0.167	0.267	0.136
Y	0.229	0.898	1.85	0.938	1.93	3.34	18.3	4.75	1.72	44.7	31.8	23.0
Zr	0.192	0.941	2.09	1.01	2.06	4.69	22.1	9.95	2.80	54.7	34.5	35.6
La (ppm)	b.d.	0.012	0.018	0.015	0.034	0.015	0.200	0.050	0.005	0.096	0.056	0.029
Ce	0.026	0.050	0.059	0.044	0.113	0.091	1.28	0.316	0.033	0.524	0.339	0.245
Nd	b.d.	0.067	0.064	0.065	0.185	0.147	2.04	0.513	0.069	0.889	0.794	0.570
Sm	b.d.	0.033	0.055	0.038	0.102	0.094	1.10	0.294	0.063	0.798	0.690	0.510
Eu	b.d.	0.007	0.019	0.007	0.025	0.015	b.d.	b.d.	0.010	0.010	0.008	0.008
Dy	0.020	0.088	0.151	0.105	0.228	0.412	2.33	0.648	0.196	5.27	3.28	2.83
Eu	0.026	0.080	0.134	0.096	0.221	0.362	1.45	0.449	0.147	5.65	2.88	2.44
Yb	0.046	0.121	0.226	0.125	0.283	0.462	1.62	0.525	0.191	9.24	3.88	3.06

Note: b.d. = below detection.

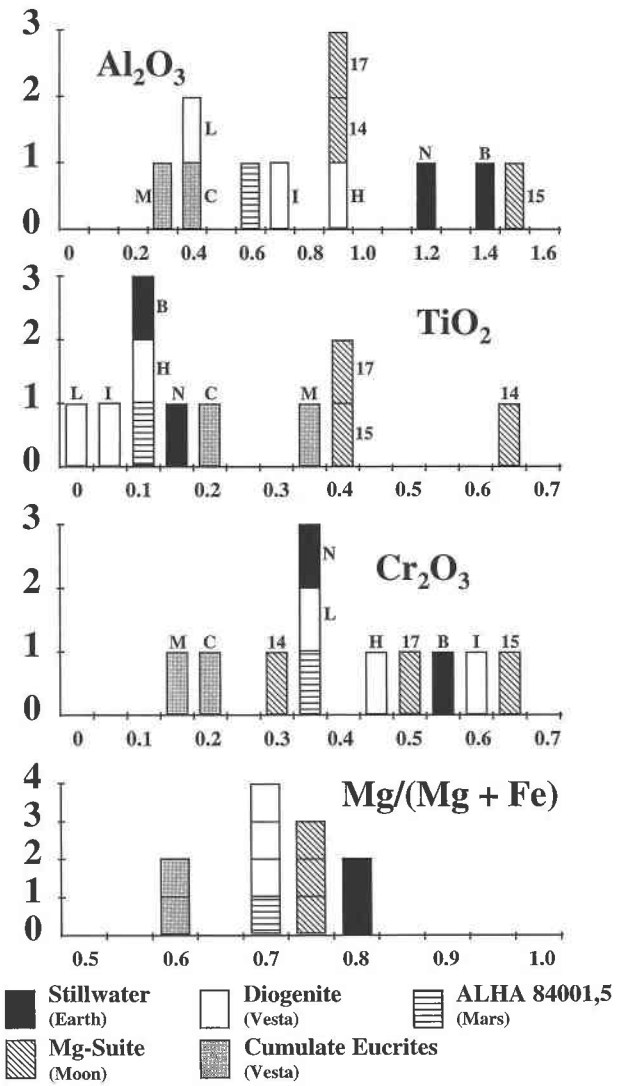

FIGURE 27. Histograms of selected chemical parameters reported in Table 3. For Stillwater samples, B = bronzitites and N = norites; for lunar Mg suite, 14 = Apollo 14, 15 = Apollo 15, and 17 = Apollo 17 site; for diogenites, L = low-Ti, I = intermediate-Ti, and H = high-Ti group; for cumulate eucrites, C = Binda, Serra de Magé, and Moama averaged, and M = Moore County.

from Stillwater norite near 0.81. With the realization that resetting of the Mg′ may have taken place, we estimate the Mg′ values of possible parental melts. The exchange coefficient K_D of Grove and Bence (1977) of 0.28 (1200 °C) was used in these calculations. Also, if we identified the parental melt composition for the Stillwater bronzitites (Table 2; 50:50 mix), then we have another estimate of orthopyroxene-melt partitioning. We calculate K_D = 0.29 using Mg'_{Opx} = 0.844 and Mg'_{melt} = 0.61. Despite the uncertainty in these estimates, clearly the Stillwater orthopyroxenite sequence crystallized from more magnesian melts than the diogenites.

Figure 24 shows that Al_2O_3 is considerably higher in orthopyroxene from Stillwater bronzitites than from diogenites. If we assume $D_{Al_2O_3}$ = 0.1 (Fowler et al. 1994), the average Al_2O_3 contents for the three groups of melts parental to diogenites (Table 3) are estimated to be 5, 7, and 10 wt% Al_2O_3, respectively. This contrasts with Al_2O_3 = 13.2 wt% for the assumed parental melt of the Stillwater bronzitites (note Table 2, 50:50 mix). Thus, it does appear that the melts parental to diogenites have lower Al_2O_3 than the parental melts of Stillwater bronzitites. Also, the CaO contents of orthopyroxene from diogenites are lower than the CaO contents of orthopyroxene from Stillwater bronzitites (Table 3). These observations are consistent with the Stolper (1977) model that predicts that melts parental to diogenites are low in normative plagioclase.

Trace elements are summarized in Table 4. As predicted from the different orthopyroxene Ca contents, the Sr contents of Stillwater orthopyroxene from bronzitites are higher than those from diogenites. Selected trace elements are compared for Stillwater bronzitites and norites and diogenites in Figures 24 and 25. There is considerable overlap in the ranges of Ti, Y, Yb, and Zr between orthopyroxene from Stillwater bronzitites and diogenites. However, it is interesting to note that the orthopyroxene from diogenites has a range that includes much lower values of the incompatible trace elements. This observation is consistent with a mantle source assemblage for diogenite parental melts that is depleted in these elements because of the proposed prior removal of eucritic basalts (Stolper 1977).

Figure 26 illustrates average chondrite-normalized orthopyroxene REE patterns for Stillwater bronzitites and norites and diogenites. Estimated parental melt REE patterns are also illustrated. The chondrite-normalized REE patterns for orthopyroxene from Stillwater bronzitites and diogenites are approximately parallel, but the diogenites plot at lower values. If the same partition coefficients are used (Lambert and Simmons 1987; Papike et al. 1995) for estimating REE in the Stillwater and diogenite parental melts, the REE plots at lower concentrations for diogenites than for the Stillwater bronzitites.

In our recent paper concerning the petrogenesis of diogenites (Fowler et al. 1995) and the discussion above, we had difficulty rationalizing the major, minor, and trace element chemistry of orthopyroxenite with any model that was completely satisfactory. The problems include a limited range of major elements, including Mg′, but a large range in concentration of incompatible minor and trace elements (e.g., Ti, Y, Zr, Yb), which is difficult to model with any reasonable crystallization scenarios. The range of trace element concentrations leads to the prediction of >90% fractional crystallization of a closed system, single-reservoir model. To add to the difficulties, no cumulus feldspar or even intercumulus feldspar (<1%) was observed in the diogenites.

Therefore, we decided to look at a well-studied terrestrial orthopyroxenite sequence to see if we could gain

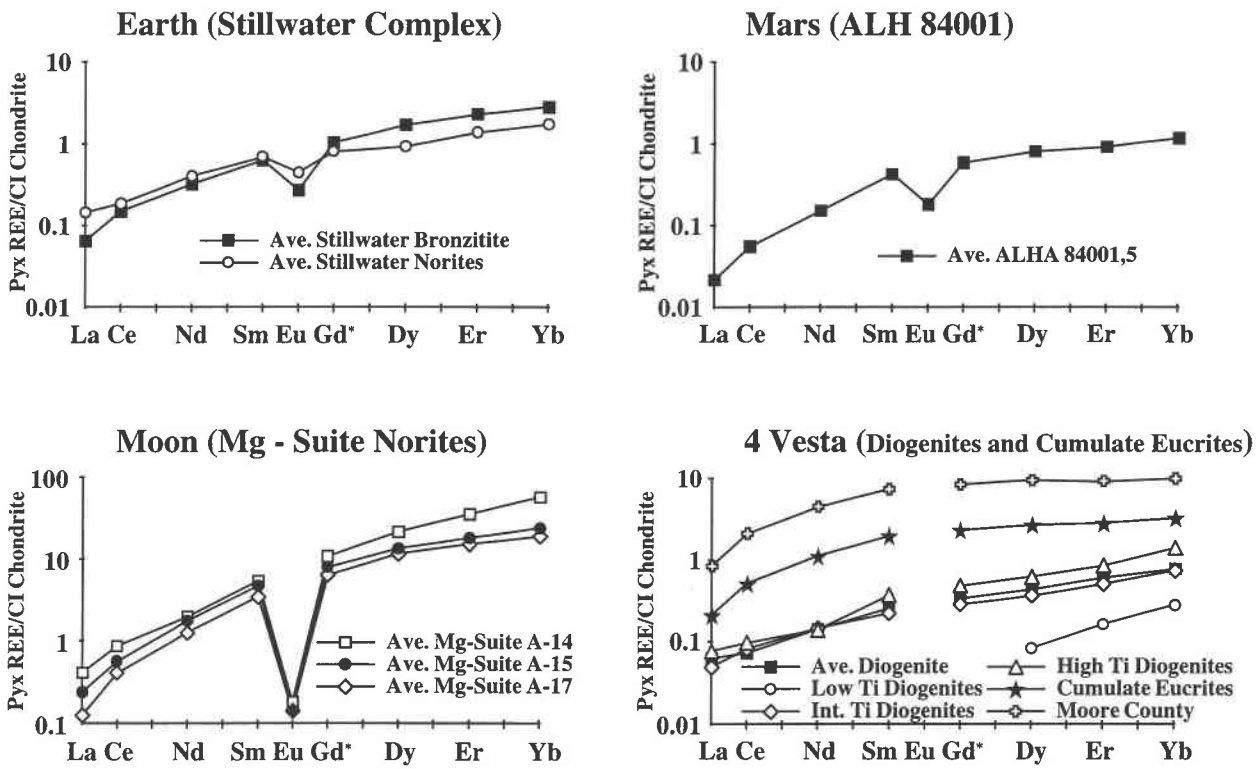

FIGURE 28. Chondrite-normalized (Anders and Grevesse 1989) REE patterns for pyroxenes. Data reported in Table 4.

some further insights about the diogenites. An attractive model for the petrogenesis of the Ultramafic series of the Stillwater Complex was presented by Helz (1992, 1995) in which she suggested that the Ultramafic series was generated by periodic influxes of two end-member magmas (mafic norite and magnesian gabbronorite, Table 2) with different trace element concentrations (Papike et al. 1995) but nearly identical Mg′ = 0.61. Figure 25 shows the range of a Ti, Y, Zr, and Yb for Stillwater bronzitites and norites and diogenites. As mentioned above, Fowler et al. (1995) showed that the observed range of Yb in diogenites, using several assumptions concerning the behavior of the partition coefficients, leads to an estimate of >90% fractional crystallization for a closed system, single-reservoir model. If we conduct identical calculations for the range of Yb for orthopyroxene from Stillwater bronzitites we calculate >60% crystallization. This is not a reasonable estimate based on previous Stillwater studies. Also, we observed no systematic variation in the concentration of the orthopyroxene incompatible trace elements with stratigraphic height in the Bronzitite zone (Fig. 23).

On the basis of the discussion above, we suggest that a model similar to that proposed by Helz (1992, 1995) be considered for the petrogenesis of diogenites. We do not believe that magnesian eucrites (e.g., Kapoeta Rho, Table 2, Bartels and Grove 1991) are parental to diogenites. Instead, we favor the model of Stolper (1977), which suggests that the melts parental to diogenites result from depleted mantle reservoirs that already experienced extraction of eucritic magmas by variable amounts of partial melting. This 4 Vesta mantle can be envisioned as having several depleted mantle reservoirs with similar major elements (e.g., Mg′) but variable incompatible trace element concentrations. These reservoirs are tapped by further melting either to form several discrete plutons or, alternatively, to form melts that may commingle (e.g., Helz 1992, 1995) and form a limited number of plutons by magma mixing. This model has the advantage of reconciling the limited range of Mg′ but very large range of incompatible trace elements.

An important lesson gained by this exercise in comparative planetology is that if simple petrogenetic models do not work for well-studied terrestrial occurrences, there is little reason to believe they will work for planetary environments in which we have little geologic control on the sampling.

MARTIAN METEORITES AND A MARTIAN ORTHOPYROXENITE

There is now considerable agreement that meteorites classified under the names Shergottite, Nahklite, and Chassignite (SNC meteorites) came from Mars (e.g., McSween 1994). This linkage to Mars is based on their young crystallization ages (which require a fairly large parent body) and a close match between the gases implanted in them during shock and the atmosphere of Mars

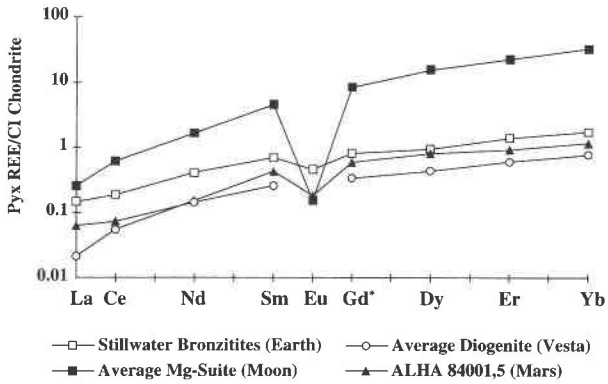

FIGURE 29. Chondrite-normalized (Anders and Grevesse 1989) pyroxene REE patterns in a summary diagram illustrating the average lunar Mg-suite norite, average diogenite (asteroid 4 Vesta), martian orthopyroxenite (ALHA 84001), and average Stillwater bronzitite (Earth).

(sampled and analyzed by the Viking landers). A comprehensive review of the martian meteorites and what they have told us about Mars is presented by McSween (1994). Shergottites can be divided into two groups: basaltic and lherzolites-harzburgites. Basaltic shergottites consist predominantly of pigeonite, augite, plagioclase, titanomagnetite, ilmenite, pyrrhotite, and whitlockite. Lherzolitic shergottites consist of olivine and chromite enclosed in large poikilitic orthopyroxene along with plagioclase, pigeonite, augite, whitlockite, and chromite filling the interstices. The nahklites are clinopyroxenites-wehrlites consisting of magnesian augite, olivine, plagioclase, alkali feldspar, pigeonite, titanomagnetite, pyrite, troilite, chalcopyrite, and chlorapatite. Chassigny is a dunite made up primarily of Fe-rich olivine with minor pigeonite, augite, alkali feldspar, chromite, troilite, marcasite, pentlandite, chlorapatite, ilmenite, rutile, and baddelyite. A new addition to the suite of martian meteorites is an orthopyroxenite (ALH 84001; Mittlefehldt 1994) that is of most relevance to the present study. It is composed mostly of magnesian orthopyroxene with subordinate amounts of plagioclase, augite, apatite, and pyrite. The shock history of this meteorite was studied by Treiman (1995a, 1995b), who believes that the meteorite experienced two major shock events. Treiman (1995b) also believes that the martian meteorites came from at least three locations on Mars. Shergottites could have been derived from one locality and the nahklites and Chassigny from a different locality. ALH 84001 appears to have come from a third locality possibly sampling ancient martian crust (Treiman 1995a, 1995b).

COMPARATIVE PLANETOLOGY

Average EMP and SIMS analyses for the diogenites, cumulate eucrites, Stillwater Complex bronzitites and norites, lunar Mg suite, and a martian orthopyroxenite are presented in Tables 3 and 4. Figure 27 presents se-

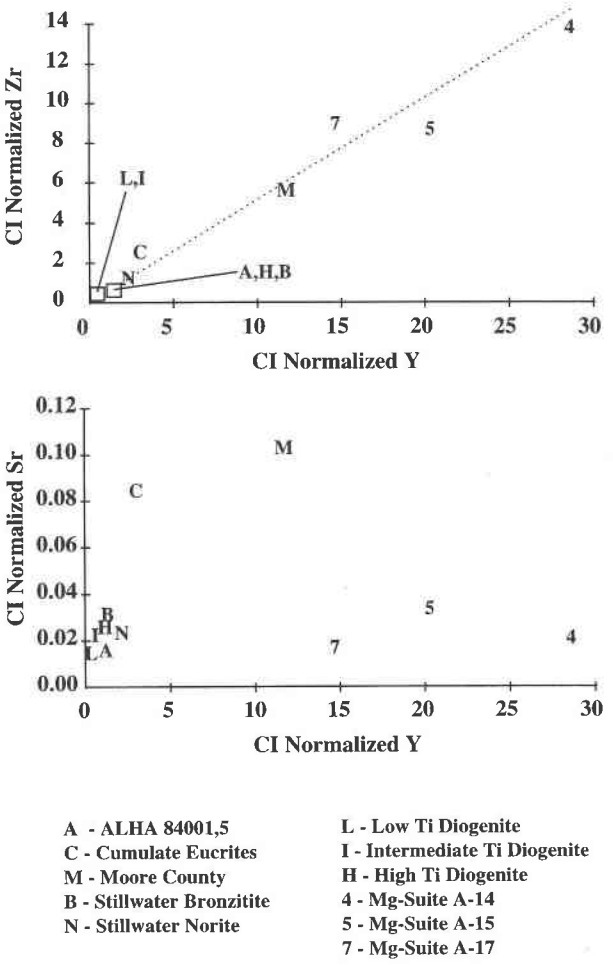

FIGURE 30. Chondrite-normalized (Anders and Grevesse 1989) Zr vs. Y and Sr vs. Y diagrams for pyroxenes. Top diagram shows a strong correlation of Zr and Y, and bottom diagram shows higher Sr values are correlated with the higher Ca in pigeonite in cumulate eucrites in comparison with lower Ca orthopyroxene in the other sample suites.

lected histograms for Al_2O_3, TiO_2, Cr_2O_3, and Mg′. Note that although cumulate eucrites are illustrated for comparative purposes, these data are for pigeonites with compositions that were reconstructed with weighted averages from analyses taken on host low-Ca pyroxenes and augite lamellae (Pun and Papike 1995). It is likely that the igneous signature was compromised by complex exsolution and reequilibration processes. Nevertheless, the much lower Mg′ for these pyroxenes in comparison with the other suites is probably significant, and if indeed the cumulate eucrites occur in the same 4 Vesta plutons as the diogenites (Fig. 7), the difference in Mg′ for the diogenites and the cumulate eucrites is perhaps larger than would be expected. Three of the cumulate eucrites we studied (Binda, Serra de Magé, and Moama) are quite similar chemically (Fig. 6), and they are grouped together and separate from Moore County, which is significantly dif-

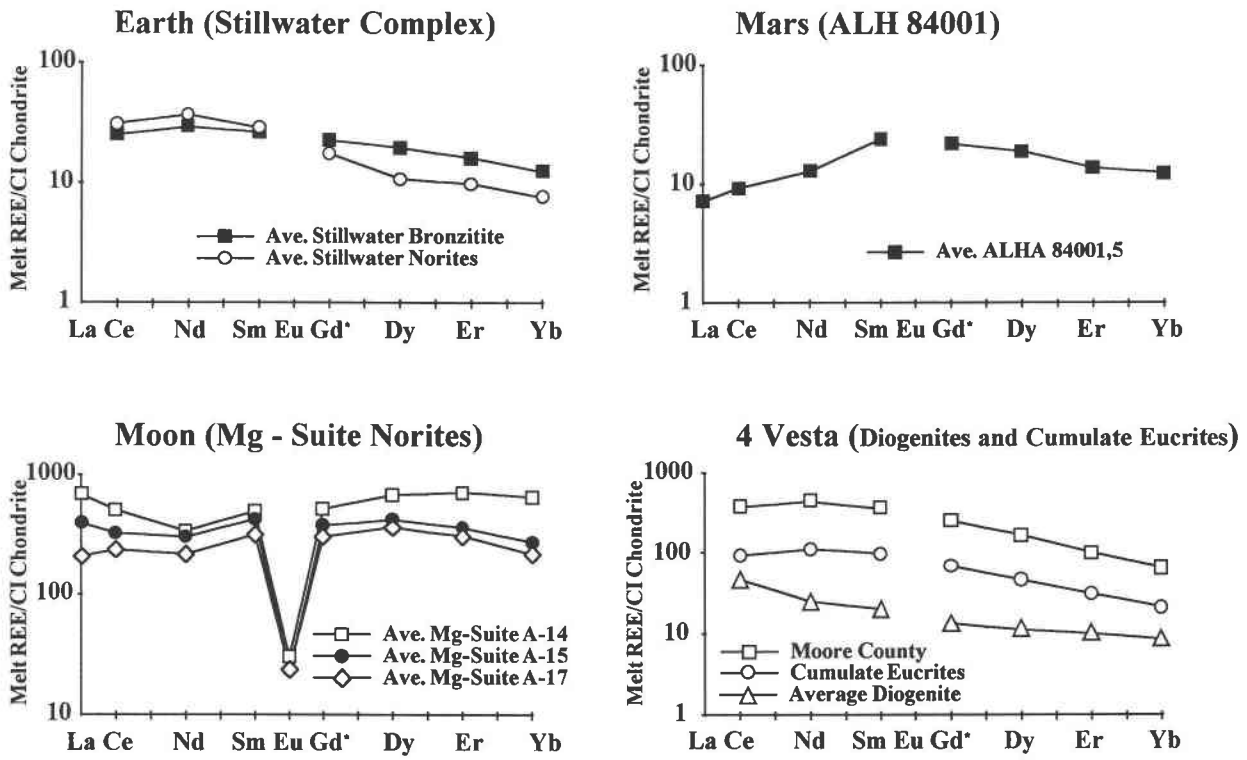

FIGURE 31. Calculated REE patterns of parental melts using partition coefficients listed in Table 5.

ferent. The diogenites and martian orthopyroxenite, ALH 84001, have similar Mg′ values, which are lower than those of either the lunar Mg suite or the Stillwater samples.

Figures 28 and 29 summarizes REE systematics for the different planetary sample suites. There are clearly some significant differences. For the asteroid 4 Vesta samples (diogenites and cumulate eucrites) we did not plot Eu because it was below detection in most of the diogenites analyzed and in the low-Ca hosts of the inverted pigeonites of the cumulate eucrites. Nevertheless, the low abundance of Eu in these pyroxenes indicates a high Eu^{2+}/Eu^{3+} ratio in the melts consistent with a low f_{O_2} (see, for example, the discussion by Jurewicz et al. 1995). Thus, although not plotted, these pyroxenes have a large negative Eu anomaly. The cumulate eucrite pyroxenes have higher REE than the diogenites, which is consistent with their being related by a fractionation sequence. However, again it must emphasized that the chemical signatures in the cumulate eucrite pyroxenes may be compromised. The orthopyroxene from the lunar Mg-suite norites shows striking REE enrichments and large negative Eu anomalies. The Apollo 14 pyroxenes show the highest REE enrichments especially for the heavy REE. Orthopyroxene from the Stillwater bronzitites and norites and martian sample ALH 84001 shows significantly smaller negative Eu anomalies consistent with higher oxygen fugacities related to magmatism on Earth and Mars.

Figure 29 compares REE from orthopyroxene (pigeonite compositions from the cumulate eucrites are not included) and illustrates the striking difference in abundance of REE in the lunar Mg-suite norites compared to the other suites. Truly planetary-scale processes had to conspire to produce these high REE abundances in orthopyroxene! First, the Moon had to melt to great depth (e.g., 800 km, Hess and Parmentier 1995; Moon's radius

TABLE 5. Orthopyroxene-melt partition coefficients used in this study

Source	La	Ce	Nd	Sm	Eu	Dy	Er	Yb
Lundberg et al. (1990)	0.003	0.006	0.012	0.018		0.043	0.068	0.095
McKay et al. (1991)	0.0006*	0.00172	0.0058	0.011	0.006*	0.032*	0.050*	0.087
McKay et al. (1991)**	0.003	0.0055	0.01	0.02		0.057	0.089	0.15
Lambert and Simmons (1987)†		0.006	0.011	0.024		0.087	0.141	0.229

* Interpolated and extrapolated values.
** Estimated for 8% WO contents of pigeonite in cumulate eucrites.
† Values given in Papike et al. (1995).

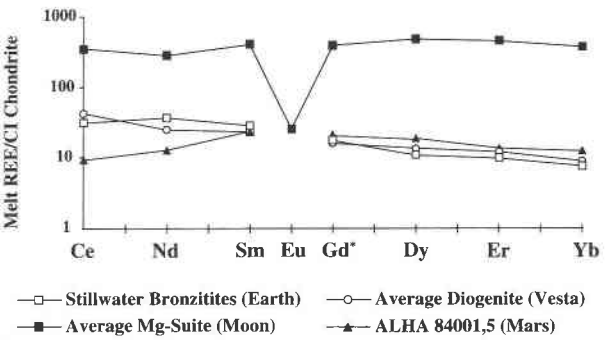

FIGURE 32. Summary diagram of calculated REE patterns of parental melts. Cumulate eucrites were excluded because trace element signatures of pyroxenes might have been compromised by subsolidus reactions.

is 1738 km) to result in these incredible enrichments. The KREEP-rich lithologies are thought to be the last dregs of the magma-ocean fractionation (see discussion above), and these lithologies are enriched in the incompatible K, REE, and P. The large negative Eu anomaly is likely the result of significant plagioclase crystallization that formed the lunar anorthosites that preceded KREEP crystallization. However, even these events were not sufficient to enrich the melts, which were parental to the Mg-suite norites, sufficiently to produce the REE signatures observed in the Mg-suite orthopyroxene (Papike et al. 1994a). Advanced crystallization (up to 55%, Snyder et al. 1995b) together with trapping of varied proportions ($\leq$20%) of instantaneous, KREEP-basalt residual liquid (Snyder et al. 1995b) were also required.

Figure 30 shows chondrite-normalized (Anders and Grevesse 1989) Zr vs. Y and Sr vs. Y diagrams for pyroxenes from the various sample suites. A strong positive correlation is observed between the two incompatible trace elements Zr and Y. The pyroxenes from the lunar Mg suite show the highest concentrations of these two elements, consistent with the highly evolved nature of these rocks. In the Sr vs. Y diagram, the Sr values plot in a rather narrow range at low concentrations for orthopyroxene with low Ca concentrations (Table 3). The cumulate eucrites (symbols C and M) contain pigeonite as the primary pyroxene, which has higher Ca and Sr.

Figure 31 presents calculated parental melts using the data in Table 4 and the partition coefficients in Table 5. Selecting the correct partition coefficients is one of the most challenging aspects of this data-inversion exercise. Those selected here are somewhat arbitrary. Many *D*s exist in the literature; however, none have been specifically determined for the cumulate rocks considered in this paper. Nevertheless, with this caveat, we present some estimated melt REE patterns for the various cumulate suites. The same disclaimer is used again for the cumulate eucrites. If the pyroxenes contain compromised REE patterns because of complex subsolidus reactions, then the inversion to melt compositions only compounds the problems. Therefore, we excluded the calculated cumulate eucrite parental melts from the summary parental melt REE diagrams (Fig. 32). Once again we see the special, highly evolved parental melt REE concentrations of the lunar Mg-suite norites relative to the other sample suites.

CONCLUDING STATEMENT

Pyroxene is more than another pretty mineralogical face. It is a powerful petrologic-geochemical recorder and is especially useful in recording parental melt characteristics. However, many pyroxenes have experienced long and difficult lives with a number of relationships and experiences. It is up to the reader of the pyroxene record to sort out the events that may have resulted in the trace element signature we now observe. A powerful approach to reading the trace element record of cumulus pyroxenes is to analyze the cores (inverted pigeonite excluded) of the cumulus grains with an ion microprobe for elements with assumed slow diffusion rates (e.g., REE, Y, Zr). I am confident that in many (most?) cumulus pyroxene grains the igneous trace element signature is still faithfully preserved. I am less confident that we are using the most appropriate partition coefficients to estimate parental melt compositions.

ACKNOWLEDGMENTS

Many people and institutions are responsible for the research that I report in this paper. The research was conducted in close collaboration with my colleagues Grant Fowler, Chip Shearer, Mike Spilde, Graham Layne, Stu McCallum, and Aurora Pun. This research would not have been possible without the expert stewardship of our ion microprobe facility by Graham Layne and our electron microprobe facility by Mike Spilde. Sarah Coulie provided excellent assistance in certain aspects of the graphics and logistics of assembling this manuscript. Special thanks goes to Grant Fowler for all aspects of this research through data acquisition (EMP and SIMS), data-display presentations and vigorous scientific discussions. An earlier draft of this paper was reviewed by my colleagues Adrian Brearley, Grant Fowler, Chip Shearer, and Mike Spilde, and I am grateful for their help. This research was directly supported by NASA grant NAGW-3347 and the Institute of Meteoritics. The UNM/SNL Ion Microprobe Facility is partially supported with a grant from the NSF (EAR-9303864, 1993–1995, and EAR-9506611, 1995–1997). To these institutions I express my sincere thanks.

REFERENCES CITED

Anders, E., and Grevesse, N. (1989) Abundances of the elements: Meteoritic and Solar. Geochimica et Cosmochimica Acta, 53, 197–214.

Barnes, S.J. (1986) The effect of trapped liquid crystallization on cumulus mineral compositions in layered intrusions. Contributions to Mineralogy and Petrology, 93, 524–531.

Bartels, K.S., and Grove, T.L. (1991) High-pressure experiments on magnesian eucrite compositions: Constraints on magmatic processes in the eucrite parent body. Proceedings of the 21st Lunar and Planetary Science Conference, 351–365.

Binzel, R.P., and Xu, S. (1993) Chips off asteroid 4 Vesta: Evidence for the parent body of basaltic achondrite meteorites. Science, 260, 186–191.

Cameron, M., and Papike, J.J. (1981) Structural and chemical variations in pyroxenes. American Mineralogist, 66, 1–50.

Consolmagno, G.J., and Drake, M.J. (1977) Composition and evolution of the eucrite parent body: Evidence from rare earth elements. Geochimica et Cosmochimica Acta, 41, 1271–1282.

Czamanske, G.K., and Zientek, M.L., Eds. (1985) The Stillwater Complex, Montana: Geology and guide, 396 p. Montana Bureau of Mines and Geology, Special Publication 92.

DePaolo, D.J., and Wasserburg, G.J. (1979) Sm-Nd age of the Stillwater Complex and the mantle evolution curve for neodymium. Geochimica et Cosmochimica Acta, 43, 999–1008.

Drake, M.J. (1979) Geochemical evolution of the eucrite parent body: Possible nature and evolution of asteroid 4 Vesta? In T. Hehrels, Ed., Asteroids, p. 765–782. University of Arizona Press, Tucson.

Dymek, R.F., Albee, A.L., Chodos, A.A., and Wasserburg, G.J. (1976) Petrography of isotopically dated clasts in the Kapoeta howardite and petrologic constraints on the evolution of its parent body. Geochimica et Cosmochimica Acta, 40, 1115–1130.

Fowler, G.W., Papike, J.J., Spilde, M.N., and Shearer, C.K. (1994) Diogenites as asteroidal cumulates: Insights from orthopyroxene major and minor element chemistry. Geochimica et Cosmochimica Acta, 58, 3921–3929.

Fowler, G.W., Shearer, C.K., and Papike, J.J. (1995) Diogenites as asteroidal cumulates: Insights from orthopyroxene trace element chemistry. Geochimica et Cosmochimica Acta, 59, 3071–3084.

Grove, T.L., and Bence, A.E. (1977) Experimental study of pyroxene-liquid interaction in quartz-normative basalt 15597. Proceedings of the 8th Lunar Science Conference, 1549–1579.

Grove, T.L., and Bartels, K.S. (1992) The relation between diogenite cumulates and eucrite magmas. Proceedings of the 22nd Lunar and Planetary Science Conference, 437–445.

Helz, R.T. (1985) Compositions of fine-grained mafic rocks from sills and dikes associated with the Stillwater Complex. In G.K. Czamanske and M.L. Zientek, Eds., The Stillwater Complex, Montana: Geology and guide, p. 96–117. Montana Bureau of Mines and Geology Special Publication 92, Butte, Montana.

——— (1992) Experimental constraints on the origin of the Ultramafic Series of the Stillwater Complex, Montana. Geological Society of America Abstracts with Programs, 24, A85–A86.

——— (1995) The Stillwater Complex, Montana: A subvolcanic magma chamber? American Mineralogist, 80, 1343–1346.

Hess, H.H. (1960) Stillwater igneous Complex, Montana: A quantitative mineralogical study. Geological Society of America Memoirs, 80, 230 p.

Hess, P.C., and Parmentier, E.M. (1995) A model for the thermal and chemical evolution of the Moon's interior: Implications for the onset of mare volcanism. Earth and Planetary Science Letters, 134, 501–514.

James, O.B. (1980) Rocks of the early lunar crust. Proceedings of the 11th Lunar and Planetary Science Conference, 365–393.

Jurewicz, A.J.G., Mittlefehldt, D.W., and Jones, J.H. (1995) Experimental partial melting of the St. Severin (LL) and Lost City (H) chondrites. Geochimica et Cosmochimica Acta, 59, 391–408.

Lambert, D.D. (1982) Geochemical evolution of the Stillwater Complex, Montana: Evidence for the formation of platinum-group element deposits in mafic layered intrusions, 274 p. Ph.D. thesis, Colorado School of Mines, Golden.

Lambert, D.D., and Simmons, E.C. (1987) Magma evolution in the Stillwater Complex, Montana: I. Rare-earth element evidence for the formation of the Ultramafic Series. American Journal of Science, 287, 1–32.

——— (1988) Magma evolution in the Stillwater Complex, Montana: II. Rare earth element evidence for the formation of the J-M Reef. Economic Geology, 83, 1109–1126.

Lambert, D.D., Walker, R.J., Morgan, J.W., Shirey, S.B., Carlson, R.W., Zientek, M.L., Lipin, B.R., Koski, M.S., and Cooper, R.L. (1994) Re-Os and Sm-Nd isotope geochemistry of the Stillwater Complex, Montana: Implications for the petrogenesis of the J-M Reef. Journal of Petrology, 35, 1717–1753.

Lundberg, L.L., Crozaz, G., and McSween, H.Y. (1990) Rare earth elements of the ALHA 77005 shergottite and implications for its parent magma and crystallization history. Geochimica et Cosmochimica Acta, 54, 2535–2547.

Mason, B. (1962) Meteorites, p. 274. Wiley, New York.

McCallum, I.S., Raedeke, L.D., and Mathez, E.A. (1980) Investigations of the Stillwater Complex: Part I. Stratigraphy and structure of the Banded Zone. American Journal of Science, 280-A, 59–87.

McKay, G. (1989) Partitioning of rare earth elements between major silicate minerals and basaltic melts. In Geochemistry and Mineralogy of Rare Earth Elements, 21, 45–74.

McKay, G., Le, L., and Wagstaff, J. (1991) Constraints on the origin of the mare basalt europium anomaly: REE Partition Coefficients for pigeonite. Lunar and Planetary Science, XXII, 883–884.

McSween, H.Y., Jr. (1994) What we have learned from Mars from SNC meteorites. Meteoritics, 29, 757–779.

Mittlefehldt, D.W. (1994) The genesis of diogenites and HED parent body processes. Geochimica et Cosmochimica Acta, 58, 1537–1552.

Papike, J.J., Fowler, G.W., and Shearer, C.K. (1994a) Orthopyroxene as a recorder of lunar crust evolution: An ion microprobe investigation of Mg-suite norites. American Mineralogist, 79, 796–800.

Papike, J.J., Fowler, G.W., Layne, G.D., Spilde, M.N., and Shearer, C.K. (1994b) ALH 84001 a "SNC orthopyroxenite": Insights from SIMS analysis of orthopyroxene and comparisons to diogenites. Lunar and Planetary Science, XXV, 1043–1044.

Papike, J.J., Spilde, M.N., Fowler, G.W., and McCallum, I.S. (1995) SIMS studies of planetary cumulates: Orthopyroxene from the Stillwater Complex, Montana. American Mineralogist, 80, 1208–1221

Phinney, W.C., Lindstrom, D.J., Mittlefehldt, D.W., and Martinez, R.R. (1993) Post-igneous redistribution of components in eucrites. Lunar and Planetary Science, XXIV, 1137–1138.

Pun, A., and Papike, J.J. (1995) Ion microprobe investigation of exsolved pyroxenes: Determination of minor and trace-element partition coefficients. Geochimica et Cosmochimica Acta, 59, 2279–2289.

Raedeke, L.D. (1982) Petrogenesis of the Stillwater Complex, 212 p. Ph.D. thesis, University of Washington, Seattle.

Raedeke, L.D., and McCallum, I.S. (1984) Investigations in the Stillwater Complex: Part II. Petrology and petrogenesis of the Ultramafic Series. Journal of Petrology, 25, 395–420.

Sack, R.O., Azeredo, W.J., and Lipschutz, M.E. (1991) Olivine diogenites: The mantle of the eucrite parent body. Geochimica et Cosmochimica Acta, 55, 1111–1120.

Schnetzler, C.C., and Philpotts, J.A. (1969) Genesis of the calcium-rich achondrites in the light of rare earth and barium concentrations. In P.M. Millman, Ed., Meteorite Research, p. 206–216. Springer-Verlag.

Shearer, C.K., Papike, J.J., Simon, S.B., and Shimizu, N. (1989) An ion microprobe study of the intracrystalline behavior of REE and selected trace-elements in pyroxene from mare basalts with different cooling and crystallization histories. Geochimica et Cosmochimica Acta, 53, 1041–1054.

Shearer, C.K., and Papike, J.J. (1993) Basaltic magmatism on the Moon: A perspective from volcanic picritic glass beads. Geochimica et Cosmochimica Acta, 57, 4785–4812.

Snyder, G.A., Neal, C.R., Taylor, L.A., and Halliday, A.N. (1994) Petrology and chemistry of the magnesian suite: Further evidence of liquid immiscibility and metasomatism in the western highlands of the Moon. Lunar and Planetary Science, XXV, 1305–1306.

Snyder, G.A., Taylor, L.A. and Halliday, A.N. (1995a) Chronology and petrogenesis of the lunar highlands alkali suite: Cumulates from KREEP basalt crystallization. Geochimica et Cosmochimica Acta, 59, 1185–1203.

Snyder, G.A., Neal, C.R., Taylor, L.A., and Halliday, A.N. (1995b) Processes involved in the formation of magnesian-suite plutonic rocks from the highlands of the Earth's Moon. Journal of Geophysical Research, Planets, 100, 9365–9388.

Spera, F.J. (1992) Lunar magma transport phenomena. Geochimica et Cosmochimica Acta, 56, 2253–2265.

Stolper, E. (1977) Experimental petrology of eucritic meteorites. Geochimica et Cosmochimica Acta, 41, 587–611.

Takeda, H., Miyamoto, M., Ishii, T., and Yanai, K. (1979) Mineralogical examination of the Yamato-75 Achondrites and their layered crust model. Proceedings of the 3rd Symposium on Antarctic Meteorites, 82–108.

Taylor, S.R., Norman, M.D., and Esat, T.M. (1993) The Mg-suite and the highland crust: An unsolved enigma. Lunar and Planetary Science, XXIV, 1413–1414.

Thurber, M.W., and McCallum, I.S. (1990) The Ultramafic series–Banded series contact in the Stillwater complex: Evidence for thermal erosion. Lunar and Planetary Science, XXI, 1254–1255.

Treiman, A.H. (1995a) A petrographic history of meteorite ALH 84001: Two shocks and an ancient age. Meteoritics, 30, 294–302.

——— (1995b) An ancient age for ALH84001: Petrographic evidence for multiple shock events. Meteoritics, 29, 542.

Warren, P.H. (1985) Origin of howardites, diogenites and eucrites: A mass balance constraint. Geochimica et Cosmochimica Acta, 49, 577–586.

——— (1989) KREEP: Major-element diversity, trace-element uniformity (almost) (extended abs.). In Workshop on the Moon in transition: Apollo 14, KREEP, and evolved lunar rocks, LPI Tech. Rep. 89-03, 149-153, Houston, Texas.

——— (1993) A concise compilation of petrologic information on possibly pristine nonmare Moon rocks. American Mineralogist, 78, 360–376.

Warren, P.H., and Jerde, E.A. (1987) Composition and Origin of Neuvo Laredo trend eucrites. Geochimica et Cosmochimica Acta, 51, 713–725.

Warren, P.H., and Kallemeyn, G.W. (1993) The ferroan-anorthositic suite, the extent of primordial lunar melting, and the bulk composition of the Moon. Journal of Geophysical Research, 87, 5445–5455.

Zellner, B., Storrs, A., and Wells, E.N. (1995) Images of Vesta with the planetary camera of the Hubble Space Telescope. Lunar and Planetary Science, XXVI, 1553–1554.

Manuscript received December 1, 1995
Manuscript accepted January 5, 1996